

1 **Comparing Secondary Organic Aerosols Schemes Implemented in Current**
2 **Chemical Transport Models and the Policy Implications of Uncertainties**

3 Ling Huang¹, Benjie Chen¹, Zi'ang Wu¹, Katie Tuite², Pradeepa Vennam², Greg
4 Yarwood^{2,*}, Li Li^{1,*}

5 ¹School of Environmental and Chemical Engineering, Shanghai University, Shanghai,
6 200444, China

7 ²Ramboll, Novato, California, 94945, USA

8 *Correspondence to:* Greg Yarwood (gyarwood@ramboll.com), Li Li
9 (lily@shu.edu.cn)

10 **Abstract**

11 Secondary organic aerosol (SOA) constitutes a major component of fine particulate
12 matter (PM_{2.5}) that models must account for to assess how human activities influence
13 air quality, climate, and public health. We characterize the current state of SOA
14 modeling by analyzing eight SOA schemes implemented in five widely used air
15 quality models: CAMx, CMAQ, GEOS-Chem, WRF-Chem and CHIMERE. We
16 performed offline calculations to compare non-aged SOA yields, the effects of SOA
17 aging processes, and the influence of NO_x conditions on yields. Our objective is to
18 understand variation rather than to identify a superior scheme. We find significant
19 discrepancies in SOA yields with the ratio of maximum to minimum non-aged yield
20 spans from 1.8 to over 1000, depending upon precursor. The impact of nitrogen oxide
21 (NO_x) conditions on SOA yields is also highly variable among schemes. While some
22 schemes include SOA aging, their treatments differ substantially, with some schemes
23 showing large increases in SOA mass, while others exhibit minimal changes. Box
24 model simulations confirmed the substantial discrepancies in predicted SOA
25 concentrations and their responses to precursor emission changes. The substantial
26 differences among current SOA schemes highlight a lack of consensus within the air
27 quality modelling community. Evaluating model simulation results using ambient
28 measurements is unlikely to resolve these discrepancies because uncertainties in SOA
29 formation and precursor emissions are deeply intertwined. The limitations of current
30 SOA schemes should be recognized and acknowledged because model choice can

31 greatly influence predicted SOA concentrations and their evolution, ultimately
32 impacting air quality forecasts, assessments, and regulatory decisions.

33 **Keywords:** Secondary organic aerosol (SOA), chemical transport model (CTM),
34 two-product, volatility basis set (VBS), SOA yields, CAMx, CMAQ, GEOS-Chem,
35 WRF-Chem, CHIMERE

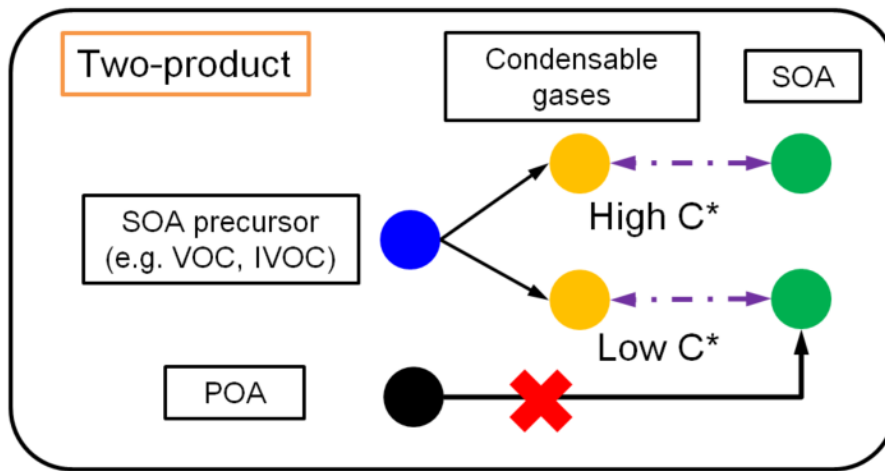
36 **1. Introduction**

37 Organic Aerosol (OA) contributes a large fraction of fine particulate matter (PM_{2.5})
38 due to primary OA emissions (POA) and the formation of secondary OA (SOA) from
39 anthropogenic, biogenic, and biomass burning sources (Donahue et al., 2006; Huang
40 et al., 2014; Tsimpidi et al., 2016). SOA precursor emissions include traditional
41 volatile organic compounds (VOC) as well as non-traditional intermediate and
42 semi-volatile VOC (IVOC and SVOC, respectively) whereas POA are directly emitted
43 from combustion sources. Recent studies report that volatile chemical products (VCPs)
44 are increasingly important contributors to SOA formation (Pennington et al., 2021;
45 Sasidharan et al., 2023). Chemical transport models (CTMs) are essential tools for
46 understanding the sources and transport of OA as well as assessing the effectiveness
47 of mitigation strategies (e.g. Pye et al., 2021; Chang et al., 2022; Chen et al., 2024;
48 Pennington et al., 2024; Vitali et al., 2024). However, accurately modeling SOA
49 formation in CTMs has posed persistent challenges due to the intricate nature of SOA
50 formation processes (Li et al., 2023). Scientific understanding of SOA formation
51 pathways is continuously evolving. Therefore, it is crucial to review the state of
52 science on SOA formation implemented in different CTMs and identify existing
53 knowledge gaps.

54 In general, CTMs adopt one of two approaches for SOA simulation: the two-product
55 scheme (Figure 1) or the volatility basis set (VBS) scheme (Figure 2a). Two-product
56 schemes apply the absorptive gas-particle partitioning theory of Pankow (1994) using
57 only two surrogate products to represent all of the condensable gases (CGs) formed
58 when SOA precursors are oxidized in the gas phase by OH radical, ozone (O₃), or
59 NO₃ radical, e.g.:

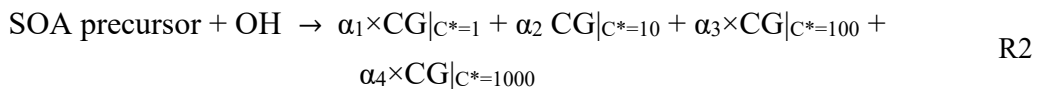


60 where CG1 and CG2 have different saturation concentration (C^*); α_1 and α_2 are molar
 61 stoichiometric yields. The α and C^* values for CG1 and CG2 are fitted to SOA
 62 formation observed in chamber experiments. SOA formation depends on the total
 63 amount of OA present (Pankow, 1994) and consequently SOA formation depends on
 64 POA. POA is usually treated as non-volatile in two-product schemes (e.g., Strader et
 65 al., 1999; Schell et al., 2001) but can be treated as semi-volatile in a modified
 66 two-product scheme (e.g. Huang et al. 2024).



67
 68 **Figure 1** Illustration of a “two-product” SOA scheme combined with a non-volatile
 69 treatment of POA

70 The VBS framework (Donahue et al., 2006) expands the two-product model by
 71 having more condensable gases that are systematically organized by volatility (i.e.,
 72 C^*). Condensable organic compounds are categorized based on their volatility into
 73 bins that are typically separated by a factor of 10, e.g., four bin with C^* of 1, 10, 100,
 74 1000 $\mu\text{g}/\text{m}^3$:



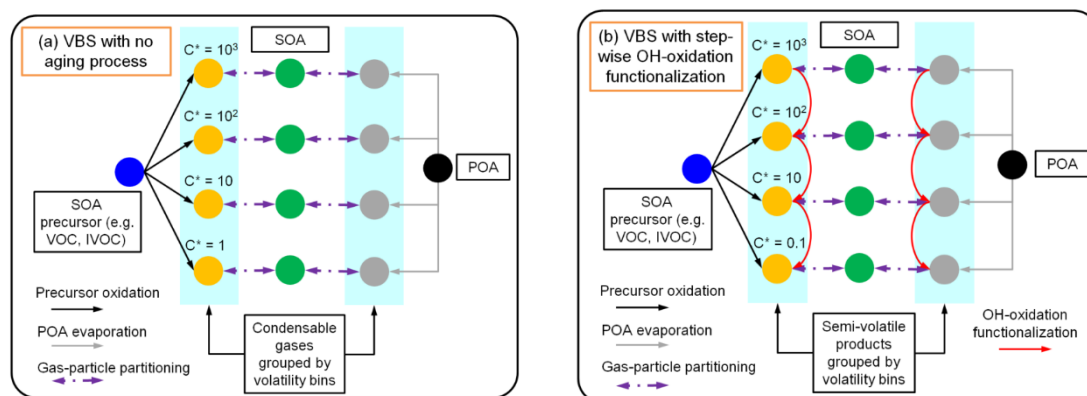
75 Similar to the two-product model, the VBS framework is based on the absorptive
 76 partitioning theory and the CG yield (α) for each volatility bin can be obtained by
 77 fitting the results of laboratory studies. Many VBS schemes treat POA as being
 78 semi-volatile and able to dynamically partition between the gas and particle phase
 79 depending on environmental factors, similar to SOA. Figure 2 illustrates the

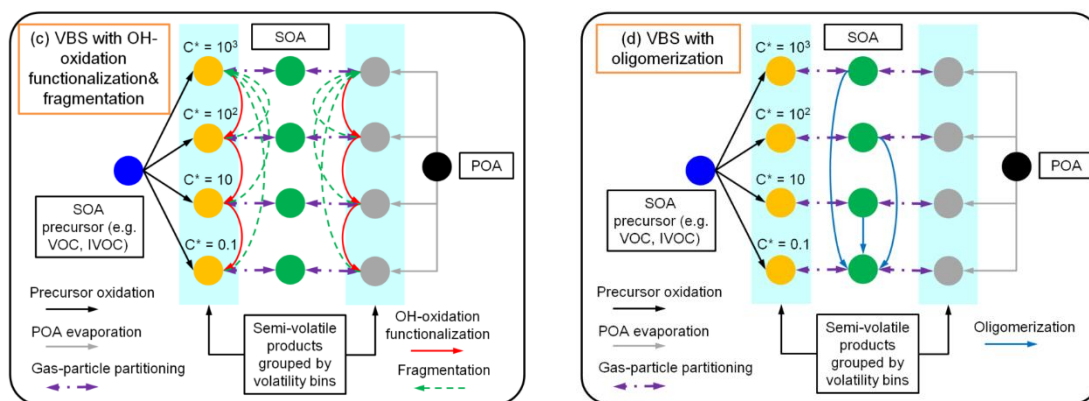
80 “1-dimensional” (1-D) VBS framework where volatility is the dimension that varies
81 (discretized to volatility bins) and panels a-d illustrate various treatments of SOA
82 aging. In the 2-D VBS introduced by Donahue et al. (2011), both volatility and
83 oxidation state can vary independently. The 1.5-D VBS introduced by Koo et al.
84 (2014) represents variations in volatility and oxidation state as a single coordinate by
85 assuming they are related.

86 Figure 2a depicts a four-bin VBS framework with no aging of OA after the initial
87 formation of SOA. Emitted SOA precursors (e.g., VOC, IVOC) undergo initial
88 gas-phase oxidation and produce four types of CGs which can immediately condense
89 to form SOA. Beyond initial oxidation, multi-generational aging processes can occur
90 and include functionalization and/or fragmentation of gas-phase CGs, oligomerization
91 of condensed-phase SOA, SOA photolysis, and heterogeneous SOA oxidation.
92 Functionalization and oligomerization typically increase SOA mass by lowering
93 volatility, whereas fragmentation and photolysis decrease SOA mass. Figure 2b
94 depicts a VBS framework incorporating a step-wise OH-oxidation functionalization
95 process as included in many VBS schemes, where CGs undergo gas-phase reactions
96 (usually parameterized as OH-oxidation) that add oxygen-containing functional
97 groups and successively lower volatility. This functionalization increases molecular
98 weight with each oxidation generation, which can be parameterized as a percentage
99 increase (usually 7.5% or 15%) to account for added oxygen (Robinson et al., 2007;
100 Shrivastava et al., 2015). Gas-phase reactions of CGs can cause molecular
101 fragmentation as well as functionalization. As SOA ages, fragmentation reactions may
102 gain significance (Cappa et al. 2012). Figure 2c shows a VBS framework with both
103 functionalization and fragmentation. In this scheme, OH-oxidation of the CGs forms
104 products across lower (due to functionalization) and higher (due to fragmentation)
105 volatility bins that are often parameterized using predefined fractions. Particle-phase
106 oligomerization, as illustrated by Figure 2d, is another SOA aging process where
107 condensed SOA molecules join together and form larger SOA molecules with
108 extremely low volatility. Some schemes refer to oligomerization as polymerization.

109 Typically, the rate of oligomerization is modeled as independent of the gas-phase
110 oxidant level.

111 Given the diverse treatments of SOA formation employed in CTMs, it is both
112 necessary and important to comprehensively understand and quantify the similarities
113 and differences among schemes/models. Direct comparisons of simulated SOA
114 concentrations across different CTMs can be both time-consuming and
115 resource-intensive. Furthermore, variations in other model configurations, such as
116 physical processes, may obscure the distinctions associated with the SOA schemes
117 themselves. To address this issue, we performed offline calculations outside the
118 selected CTMs to focus on SOA formation and aging processes, as described in
119 Section 2. Details of each SOA model/scheme reviewed are presented in Section 3.
120 Section 4 provides a comparative analysis of the non-aged SOA yields from typical
121 precursors as simulated by each model/scheme. Furthermore, we explore how SOA
122 aging is treated by different schemes and how NO_x conditions impact SOA yields.
123 Results from this study underscore the variability in SOA yields and highlight the
124 need for careful consideration of model selection and application in the context of air
125 quality studies.





126 **Figure 2** Illustration of VBS schemes with alternative treatments of aging: (a)
 127 no aging; (b) with step-wise OH oxidation causing functionalization only; (c) with
 128 OH-oxidation causing both functionalization and fragmentation; and (d) with
 129 condensed-phase oligomerization.

130 2. Methods

131 2.1 CTMs and SOA schemes reviewed

132 To understand the current state of SOA modelling in CTMs, we reviewed schemes
 133 implemented in several regional models that are used in the U.S., Europe, and Asia as
 134 well as one global model. We review eight SOA schemes implemented in five models,
 135 namely the Comprehensive Air Quality with Extensions (CAMx,
 136 <https://www.camx.com/>, accessed on Feb 15th, 2024), the Community Multiscale Air
 137 Quality (CMAQ, <https://github.com/USEPA/CMAQ/>, accessed on Feb 15th, 2024),
 138 GEOS-Chem (<https://geos-chem.readthedocs.io/en/stable/>, accessed on Feb 15th,
 139 2024), WRF-Chem (<https://ruc.noaa.gov/wrf/wrf-chem/>, accessed on Feb 15th, 2024),
 140 and CHIMERE (<https://www.lmd.polytechnique.fr/chimere/docs/>, accessed on Feb
 141 15th, 2024). For each model/scheme (hereafter “scheme” for simplicity), we reviewed
 142 the official documentation (e.g., user’s guide), peer-reviewed publications, and, in
 143 some cases, the model source code to understand each SOA parameterization and
 144 gather parameter data. A comparative overview of the SOA schemes is presented in
 145 Table 1 while comprehensive details regarding their specific parameterizations can be
 146 found in Section S1 of the Supporting Information.

147 The review of these SOA schemes reveals diverse parameterizations ranging from
 148 simplified, non-volatile assumptions to complex, multi-dimensional volatility basis
 149 sets. CAMx offers two distinct approaches: the SOAP2 scheme (based on Strader et

150 al., 1999) and the 1.5-D VBS (Koo et al., 2014). SOAP2 has non-volatile POA and a
151 two product SOA scheme (Figure 1) with yields fitted to the aged VBS scheme of
152 Hodzic et al. (2016), effectively treating aging as implicit. The 1.5-D VBS treats POA
153 as semi-volatile and explicitly models gas-phase aging for anthropogenic and
154 intermediate volatility precursors via OH-oxidation (Figure 2b), although this
155 stepwise aging is disabled for biogenic precursors to prevent aerosol mass
156 overprediction. The CMAQ model also provides alternative schemes: the established
157 AERO7 scheme (Appel et al., 2021) and the newer CRACMM scheme (Pye et al.,
158 2023). AERO7 utilizes a 1-D VBS framework for POA and SOA that incorporates
159 aging primarily through particle-phase processes (Figure 2d), specifically the
160 oligomerization of anthropogenic and biogenic precursors and the hydrolysis of
161 organic nitrates derived from monoterpenes. CRACMM also utilizes a 1-D VBS
162 framework for POA and SOA and simulates aging through sequential gas-phase
163 oxidation reactions involving functionalization and/or fragmentation (Figure 2c; Pye
164 et al., 2023). GEOS-Chem includes a “Simple” scheme that treats SOA as non-volatile
165 with fixed yields that are linked to ambient measurements, alongside a “Complex”
166 1-D VBS scheme without additional aging processes (Figure 2a; Pai et al., 2020).
167 CHIMERE’s 1-D VBS scheme is notable for its comprehensive aging scheme with
168 functionalization, fragmentation, and oligomerization (Figure 2d) where oxidation
169 products are redistributed across volatility bins (CHIMERE, 2023). The WRF-Chem
170 MOSAIC scheme employs a 1-D VBS for most VOCs but applies a specific stepwise
171 gas-phase aging mechanism exclusively to IVOCs (Shrivastava et al. 2011).
172 Despite these structural differences, the schemes share foundational similarities,
173 particularly in the reliance on absorptive partitioning theory by most schemes. With
174 the exception of the GEOS-Chem Simple scheme, which assumes irreversible
175 condensation, all models utilize either a two-product or VBS framework to describe
176 the equilibrium partitioning of semi-volatile organic compounds. However, the
177 treatment of aging remains the most significant source of divergence. Approaches
178 vary from neglecting aging entirely (GEOS-Chem Complex, CAMx SOAP2) to

179 implementing distinct mechanisms such as gas-phase oxidation (CAMx VBS, CMAQ
180 CRACMM) versus particle-phase oligomerization (CMAQ AERO7). Additionally, the
181 representation of IVOCs varies substantially, ranging from omission from the
182 GEOS-Chem Simple scheme, a single lumped IVOC in most schemes, and several
183 lumped IVOCs in the CRACMM scheme.

184 **2.2 Offline calculation of non-aged SOA yields**

185 The direct comparison of simulated SOA concentrations across different schemes
186 through conducting full simulations is time-consuming and uncertain because
187 configuring all models consistently is challenging. Furthermore, differences in the
188 non-SOA physical and chemical processes between models may obscure the
189 distinctions attributable specifically to the SOA schemes themselves. To address this
190 issue, an offline calculation (Huang et al., 2023, 2024) is employed to compare the
191 non-aged SOA yield (i.e., prior to any aging effects) associated with different
192 precursors across various schemes. For a two-product scheme, the non-aged SOA
193 yield (Y) is calculated by combing the gas-particle partitioning theory with the
194 stoichiometric coefficients α_i :

$$Y = \frac{\alpha_1}{1 + C_1^*/C_{OA}} + \frac{\alpha_2}{1 + C_2^*/C_{OA}} \quad \text{Eq. 1}$$

195 where C_{OA} is the total ambient concentration of organic compounds (i.e., POA + SOA)
196 and α_1 , α_2 , C_1^* , and C_2^* represent the stoichiometric coefficients and the effective
197 saturation concentrations of the above two products, which is obtained by fitting the
198 results of laboratory studies. Similarly, for a four-bin VBS scheme with no aging
199 effects, the SOA yield is calculated as:

$$Y = \frac{\alpha_1}{1 + 1/C_{OA}} + \frac{\alpha_2}{1 + 10/C_{OA}} + \frac{\alpha_3}{1 + 100/C_{OA}} + \frac{\alpha_4}{1 + 1000/C_{OA}} \quad \text{Eq. 2}$$

200 where α_i is the non-aged oxidation yield for each volatility bin i ($i=1,2,3,4$). Utilizing
201 either Eq. 1 or Eq. 2, the SOA yields under high- and low-NO_x conditions can be
202 determined at 298 K and total OA concentrations ranging from 0.1 $\mu\text{g}/\text{m}^3$ to 50 $\mu\text{g}/\text{m}^3$,
203 using the stoichiometric coefficients provided by each scheme (see detailed
204 parameters in Section S1 of the Supporting Information).

Table 1 Summary of SOA schemes implemented in CTMs reviewed in this study^a

| Model (version) | SOA scheme | SOA precursors | Aging treatment | POA treatment | SOA photolysis | References |
|----------------------|---------------|--|--|---|---|--|
| CAMx v7.20 | SOAP2 | BENZ/TOL/XYL ISOP/TERP/SESQ IVOC | No aging effect | Non-volatile, no further reactions | Photolysis rate parameterized as 0.1% of the NO ₂ photolysis rate (J _{NO2}). | Ramboll (2022) Koo et al. (2014) |
| | 1.5D VBS | | Gas-phase OH-oxidation aging for SOA formation from AVOC and IVOC | Semivolatile; gas-phase undergoes further oxidation | | |
| CMAQ v5.4 | AERO7 | BENZ/TOL/XYL ISOP/TERP/SESQ IVOC | Particle-phase of semivolatile products forms oligomers; products generated by TERP + NO ₃ undergo hydrolysis to form low-volatile products. | Semivolatile; gas-phase undergoes further oxidation | N/A | https://github.com/ USEPA/CMAQ |
| | CRACMM | BENZ/TOL/XYM/XYE APIN/LIM/SESQ IEPOX IVOC | OH oxidation aging resulting in functionalization and fragmentation based on modified 2-D VBS framework | Semivolatile; gas-phase undergoes further oxidation | N/A | Pye et al. (2023) |
| GEOS-Chem v14.3.0 | Simple | ISOP/TERP/SESQ Anthropogenic precursor scaled based on CO emissions | No aging effect | Non-volatile; 50% of POA is directly emitted; 50% is formed with a lifetime of 1.15 days, without dependence on local oxidation levels. | Described in literature but not found in source code | Pai et al. (2020), Pye et al. (2010) https://geos-chem.r eadthedocs.io/en/st able/ |
| | Complex | BENZ/TOL/XYL IVOC ISOP/MTPO LIMO/SESQ | | Semivolatile; gas-phase undergoes further oxidation with OH to form oxidized POA with lower volatility. | | |

| Model (version) | SOA scheme | SOA precursors | Aging treatment | POA treatment | SOA photolysis | References |
|--------------------|---------------|---|--|--|--|--|
| CHIMERE v2023 | VBS | ARO1/ARO2 ALK4/ALK5 OLE1/OLE2 IVOC ISOP/TERP/HUMULE | OH oxidation aging with both functionalization and fragmentation; aerosol phase undergoes oligomerization to form non-volatile products. | Semivolatile; gas-phase undergoes further oxidation. | N/A | Zhang et al. (2013); Shrivastava et al. (2015); Couvidat et al. (2018); CHIMERE (2023) |
| WRF-Chem v4.4 | MOSAIC | ALK4/ALK5 ARO1/ARO2 OLE1/OLE2 IVOC ISOP/TERP/SESQ | No aging for AVOC and BVOC; gas-phase OH-oxidation of IVOC with 15% of mass added for each generation; no fragmentation. | Semivolatile; gas-phase undergoes further oxidation | Described in literature (Zawadowicz et al. 2020) but turned off in source code | Shrivastava et al. (2011) |

^a See abbreviations in Supporting Information

135 The non-aged SOA yield Y is always calculated as mass-based in this study while the
 136 stoichiometric coefficients α_i could either be expressed in mass-base (g/g) or molar-base
 137 (ppm/ppm). An illustrative calculation is provided in the Section of S2 of the Supporting
 138 Information, with calculation spreadsheet publicly available (see Data Availability section).
 139 The non-aged SOA yields for CMAQ CRACMM are calculated slightly differently (details
 140 presented in Section S3 of the Supporting Information), given its special treatment of
 141 partially combining gas-phase chemistry and SOA formation. Our analysis included
 142 calculations for anthropogenic precursors (benzene, toluene, and xylene), IVOC and biogenic
 143 precursors (isoprene, monoterpene, and sesquiterpenes).

144 **2.3 The effect of SOA aging**

145 Some schemes, such as CAMx two-product and GEOS-Chem Simple, do not account for
 146 SOA aging while others adopt varying approaches to represent the aging process (for a
 147 comprehensive discussion, refer to Section 3). For schemes that include aging effects, we
 148 calculated the aged SOA yields for each precursor at a given time t by summing over the
 149 particle fraction of all the relevant volatility bins (i) using Eq. 3:

$$\text{Aged SOA yields}|_t = \sum_n (f_{particle}^i \cdot \text{SOA mass}|_t^i) \quad \text{Eq. 3}$$

150 where $f_{particle}^i$ is the particle-phase fraction of each volatility bin (calculated based on Eq. 4)
 151 and $\text{SOA mass}|_t^i$ is the bin total SOA mass (gas-phase + particle-phase) at time t ; n is the
 152 total number of bins.

$$f_{particle}^i = \frac{1}{1 + C_i^*/C_{OA}} \quad \text{Eq. 4}$$

153 For gas-phase OH-oxidation style aging (e.g., Figure 2b and 2c), the SOA mass is stepped
 154 through time ($\Delta t = t - (t-1)$) as follows:

$$\begin{aligned} \text{SOA mass}|_t^i = & \text{SOA mass}|_{t-1}^i \times (f_{particle}^i + f_{gas}^i \cdot e^{-k_{OH}^*[OH]^*\Delta t}) + \\ & \sum_n [\text{SOA mass}|_{t-1}^k \times f_{gas}^k \cdot (1 - e^{-k_{OH}^*[OH]^*\Delta t}) \times \alpha_k^i] \end{aligned} \quad \text{Eq. 5}$$

155 The first term on the right hand side is the SOA mass in volatility bin (i) from the previous
 156 time step ($t-1$) multiplied by the fractions that remain after Δt in the particle-phase ($f_{particle}^i$)

157 and gas-phase ($f_{gas}^i \cdot e^{-k_{OH} \cdot [OH] \cdot \Delta t}$; $f_{gas}^i = 1 - f_{particle}^i$) considering OH-oxidation. The
 158 second term is the SOA mass gain from OH-oxidation summed across all n volatility bins.
 159 Here, α_k^i is the mass yield coefficient from bin k to bin i and the term $f_{gas}^k \cdot (1 - e^{-k_{OH} \cdot [OH] \cdot \Delta t})$
 160 is the gas-phase fraction of SOA in bin k oxidized by OH during Δt .
 161 For particle-phase oligomerization-style aging (e.g. Figure 2d and the CMAQ AERO7
 162 scheme), the aged SOA yield includes the mass of a non-reactive and non-volatile oligomer
 163 bin (OLIG) in addition to the semi-volatile bins:

$$\text{Aged SOA yield}|_t = \sum_n (f_{particle}^i \cdot \text{SOA mass}|_t^i) + \text{SOA mass}|_t^{OLIG} \quad \text{Eq. 6}$$

164 The SOA mass (gas-phase + particle-phase) in each volatility bin (i) steps through time
 165 following Eq. 7 and the mass of the non-volatile oligomer bin ($\text{SOA mass}|_t^{OLIG}$) grows with
 166 mass-transfer from semi-volatile bins according to Eq. 8:

$$\text{SOA mass}|_t^i = \text{SOA mass}|_{t-1}^i \times (f_{gas}^i + f_{particle}^i \cdot e^{-k_{OLIG} \cdot \Delta t}) \quad \text{Eq. 7}$$

$$\begin{aligned} \text{SOA mass}|_t^{OLIG} = & \text{SOA mass}|_{t-1}^{OLIG} + \\ & \sum_n \{ \text{SOA mass}|_{t-1}^i \cdot f_{particle}^i \cdot (1 - e^{-k_{OLIG} \cdot \Delta t}) \cdot \beta^i \} \quad \text{Eq. 8} \end{aligned}$$

167 k_{OLIG} is the oligomerization rate and β^i is the mass yield coefficient from bin i to the
 168 non-volatile bin OLIG.

169 To compare the aging effects of different schemes, we applied Eq. 3 to Eq. 8 for one day of
 170 aging with an OH concentration of 3×10^6 molecules/cm³ with k_{OH} and/or k_{OLIG} for each
 171 scheme when applicable. A time step (Δt) of 0.2 hr was used. Any additional calculations and
 172 assumptions associated with each scheme are further described below.

173 **2.4 Box model tests based on different SOA schemes**

174 We implemented three updated SOA schemes in CAMx and performed 2-layer box modeling
175 of two locations with varied anthropogenic emissions to quantify how differences between
176 schemes can influence predicted SOA concentrations and their response to emission changes.
177 The alternate SOA schemes use the existing CAMx SOAP2 code with updated SOA yield
178 parameters so that model results clearly depend on yield assumptions rather than scheme
179 formulation or coding. Two regions of Texas were selected to capture contrasting emission
180 environments: Dallas-Fort Worth (DFW), a major urban area dominated by anthropogenic
181 emissions (e.g., aromatics and IVOCs), and Tyler (TYL), a rural area in Northeast Texas
182 characterized by high biogenic activity. The box model has a surface layer and a residual
183 layer with time-varying surface layer depth to provide a simple representation of pollutant
184 accumulation, carry-over, and diurnal variation. Simulations were conducted over a 5-day
185 period, utilizing meteorological inputs and initial conditions derived from the Texas
186 Commission on Environmental Quality (TCEQ) 2019 3-D CAMx modeling platform (TCEQ,
187 2022).

188 We implemented three new SOA schemes into CAMx that emulate SOA yields produced by
189 the CMAQ AERO7, CMAQ CRACMM and Simple schemes. Each scheme was implemented
190 by updating the yield parameters used by the CAMx SOAP2 scheme. For the CMAQ AERO7
191 and CRACMM schemes, yield curves were fitted to the respective data (Figure S3) for each
192 SOA precursor. These yields were mapped to the volatility bins defined by CAMx SOAP2 to
193 obtain the corresponding molar-based stoichiometric coefficients (Table S11-S14). Like the
194 GEOS-Chem Simple scheme, the CAMx Simple scheme treats SOA as non-volatile with
195 fixed yields that are based on multi-model averages and work by Seltzer et al. (2021).
196 Detailed descriptions of the fitting procedures, updated Simple yields, and box model
197 configurations are provided in the Section S3 of the Supporting Information.

198 We further investigate the response of SOA concentrations to varying anthropogenic VOC
199 and NO_x emissions by performing a matrix of 100 simulations for each location and SOA
200 scheme. This approach allows for a comparison of scheme performance across a wider range
201 of atmospheric concentrations and VOC/NO_x ratios. Anthropogenic emissions in the

202 sensitivity runs were based on weekday rates, while the biogenic emissions remained
203 unscaled and varied by date, consistent with the base case simulations. Anthropogenic VOC
204 emissions were scaled from 0.1 to 1.0 (in increments of 0.1), while anthropogenic NO_x
205 emissions were scaled from 0 to 9 (in increments of 1) which caused oxidant production to
206 transition between NO-limited and VOC-limited conditions. An additional simulation with a
207 50% reduction in NO_x emissions was conducted to examine SOA response to NO_x abatement,
208 which is a critical consideration for current and future air quality planning.

209 **3. Results**

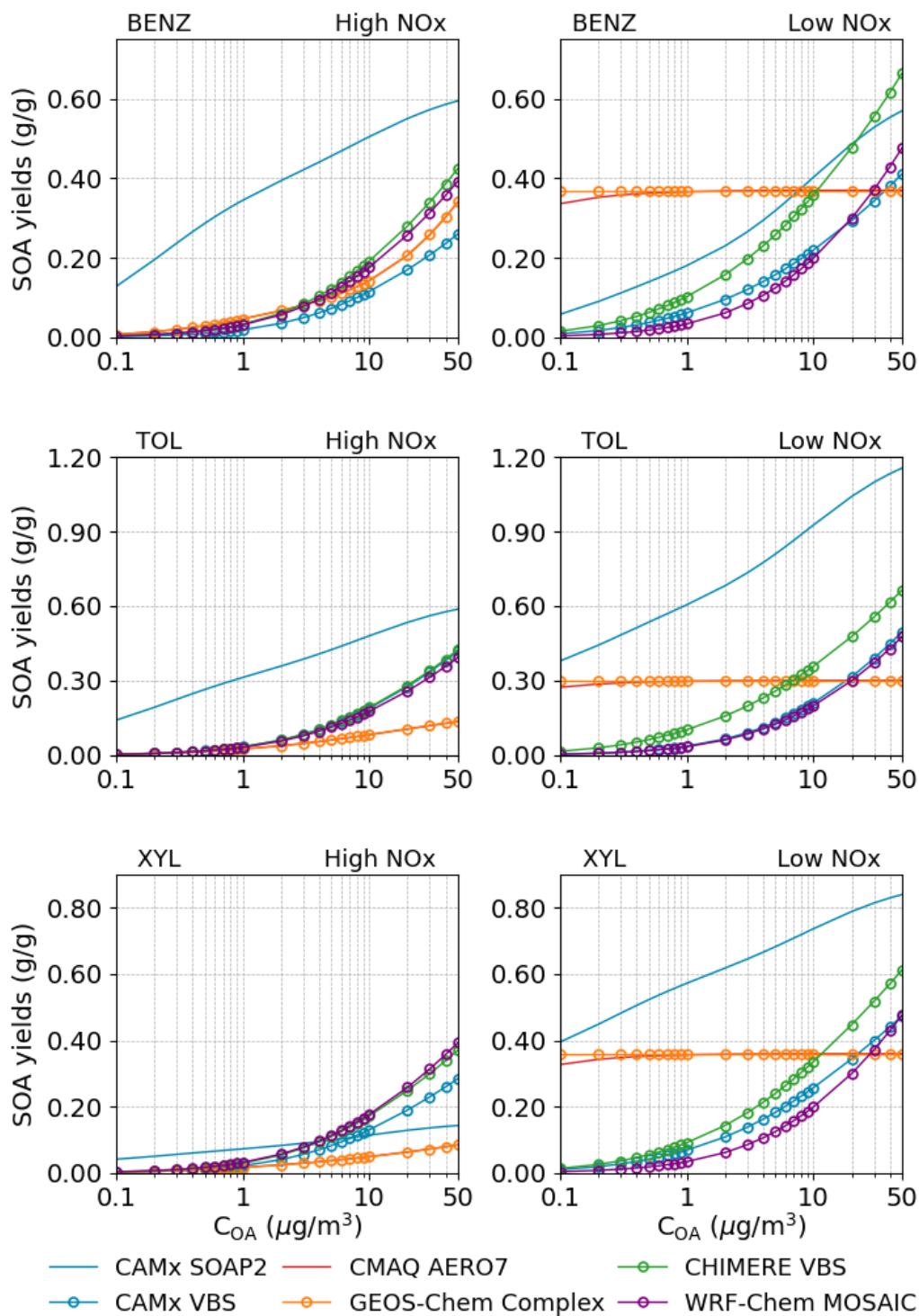
210 **3.1 Comparison of non-aged SOA yields**

211 Non-aged SOA mass yields (g/g) for all schemes (except CMAQ CRACMM) are
212 summarized in Table 2. Non-aged refers to the yields immediately following precursor
213 oxidation and before any subsequent SOA aging process. Since mass yields can vary with
214 C_{OA}, we assume C_{OA} of 10 μg/m³ in Table 2, which is relevant to ambient air quality and
215 often used as a reference C_{OA} for SOA yield comparisons. The ratio of maximum to
216 minimum non-aged SOA yields for a same precursor shows wide variations across different
217 schemes, with the least variation (factor of 1.8) observed for monoterpene at low NO_x
218 conditions and over three orders of magnitude for IVOC (factor of 3715). These variations
219 can become greater when C_{OA} is either increased or decreased from 10 μg/m³ (as assumed for
220 Table 2) and when effects of aging processes on non-aged yields are included (as shown in
221 Section 4.2).

222 **3.1.1 Non-aged SOA yields from anthropogenic VOC**

223 Figure 3 shows how the non-aged SOA mass yields depend on C_{OA} for three anthropogenic
224 VOC (AVOC), namely benzene (BENZ), toluene (TOL), and xylene (XYL). For WRF-Chem
225 and CHIMERE, the SOA yields for model species ARO1 are used to represent BENZ and
226 TOL whereas those of ARO2 are used for XYL. As illustrated by Figure 3, the SOA yields
227 from aromatics generally increase with C_{OA}, except for GEOS-Chem Simple. The SOA
228 yields become independent of C_{OA} when the product is treated as non-volatile as exemplified
229 by the GEOS-Chem Simple scheme, which assumes constant SOA yields of 100% for all
230 three precursors. Conversely, the SOA yields increase strongly with C_{OA} when the SOA is

231 treated as semi-volatile. The CAMx SOAP2 scheme is an intermediate case with SOA yields
232 increasing more gradually with C_{OA} than the CHIMERE scheme. CMAQ AERO7 and
233 GEOS-Chem Complex predict almost identical SOA yields (due to close stoichiometric
234 coefficients) and exhibit no dependence on C_{OA} under low NO_x conditions. Overall, schemes
235 consistently show higher ASOA yields from aromatics under low NO_x than high NO_x
236 conditions but diverge in the magnitude of these yields (max./min. yields at $10 \mu\text{g}/\text{m}^3$ ranging
237 from 2.0 to 5.8) and diverge in how yields depend on C_{OA} (ranging from independent to
238 strongly increasing).



239

240 **Figure 3** Comparison of the non-aged SOA yields (g/g) as functions of C_{OA} for three
 241 anthropogenic VOC among different schemes (CMAQ CRACMM not included). SOA
 242 yields are calculated at 298 K. Note that y-axis scales vary by precursor to highlight scheme
 243 discrepancies across different yield magnitudes.

244 **Table 2** Non-aged SOA yields (g/g) for different precursors across schemes at 298 K and C_{OA}
 245 of $10 \mu\text{g}/\text{m}^3$.

| Precursor- NOx case | CMx ¹ SP2 | CMx VBS | CMQ AE7 | CMQ CRM | G-C Spl | G-C Cpx | CMR VBS | W-C MOS | Avg ⁷ | Max/ Min ⁸ |
|-------------------------|-------------------------|------------|------------|------------|------------|------------|--------------------------|--------------------------|------------------|--------------------------|
| BENZ ² -high | 0.51 | 0.12 | 0.14 | 0 | / | 0.14 | 0.19 | 0.18 | 0.21 | 4.4 |
| BENZ-low | 0.40 | 0.22 | 0.37 | 0 | / | 0.37 | 0.36 | 0.20 | 0.32 | 2.0 |
| TOL ³ -high | 0.48 | 0.19 | 0.08 | 0 | / | 0.08 | 0.19 | 0.18 | 0.20 | 5.8 |
| TOL-low | 0.93 | 0.21 | 0.30 | 0 | / | 0.30 | 0.36 | 0.20 | 0.38 | 4.6 |
| XYL ⁴ -high | 0.11 | 0.13 | 0.05 | 0 | / | 0.05 | 0.17 | 0.18 | 0.12 | 3.6 |
| XYL-low | 0.74 | 0.26 | 0.36 | 0 | / | 0.36 | 0.34 | 0.20 | 0.38 | 3.7 |
| IVOC ⁵ high | 0.36 | 0.51 | 1.00 | 0 | / | 0.20 | 2.7× 10 ⁻⁴ | 2.7× 10 ⁻⁴ | 0.35 | 3715 |
| IVOC-low | 0.55 | 0.51 | 1.00 | 0 | / | 0.73 | 2.7× 10 ⁻⁴ | 2.7× 10 ⁻⁴ | 0.46 | 3715 |
| ISOP-high | 0.05 | 0.01 | 0.05 | 0 | 0.03 | 0.04 | 0.04 | 0.01 | 0.03 | 4.0 |
| ISOP-low | 0.09 | 0.03 | 0.05 | 0 | 0.03 | 0.04 | 0.07 | 0.02 | 0.05 | 3.8 |
| TERP-high | 0.14 | 0.09 | 0.17 | 0 | 0.10 | 0.09 | 0.13 | 0.10 | 0.12 | 1.8 |
| TERP-low | 0.21 | 0.18 | 0.17 | 0 | 0.10 | 0.19 | 0.25 | 0.18 | 0.18 | 2.5 |
| SESQ ⁶ -high | 0.52 | 0.22 | 0.44 | 0 | 0.10 | 0.84 | 0.20 | 0.22 | 0.36 | 8.4 |
| SESQ-low | 0.70 | 0.22 | 0.44 | 0 | 0.10 | 0.42 | 0.20 | 0.22 | 0.33 | 7.0 |

246 ¹ Model name abbreviations are CMx for CAMx, CMQ for CMAQ, G-C for GEOS-Chem, CMR for
 247 CHIMERE, and W-C for WRF-Chem. Scheme name abbreviations are SP2 for SOAP2, AE7 for AERO7, Spl
 248 for Simple, Cpx for Complex, and MOS for MOSAIC.

249 ² For WRF-Chem and CHIMERE, results for BENZ are based on ARO1.

250 ³ For WRF-Chem and CHIMERE, results for TOL are based on ARO1.

251 ⁴ For WRF-Chem and CHIMERE, results for XYL are based on ARO2. For CMAQ CRACMM, results for
 252 XYL are averages of XYE and XYM.

253 ⁵ For CMAQ CRACMM, IVOC yields are average of alkane and oxygenated IVOCs (see details in Table S17).
 254 For WRF-Chem MOSAIC, IVOC is assumed to have 50% oxygen.

255 ⁶ For CHIMERE, results for SESQ are based on humulene.

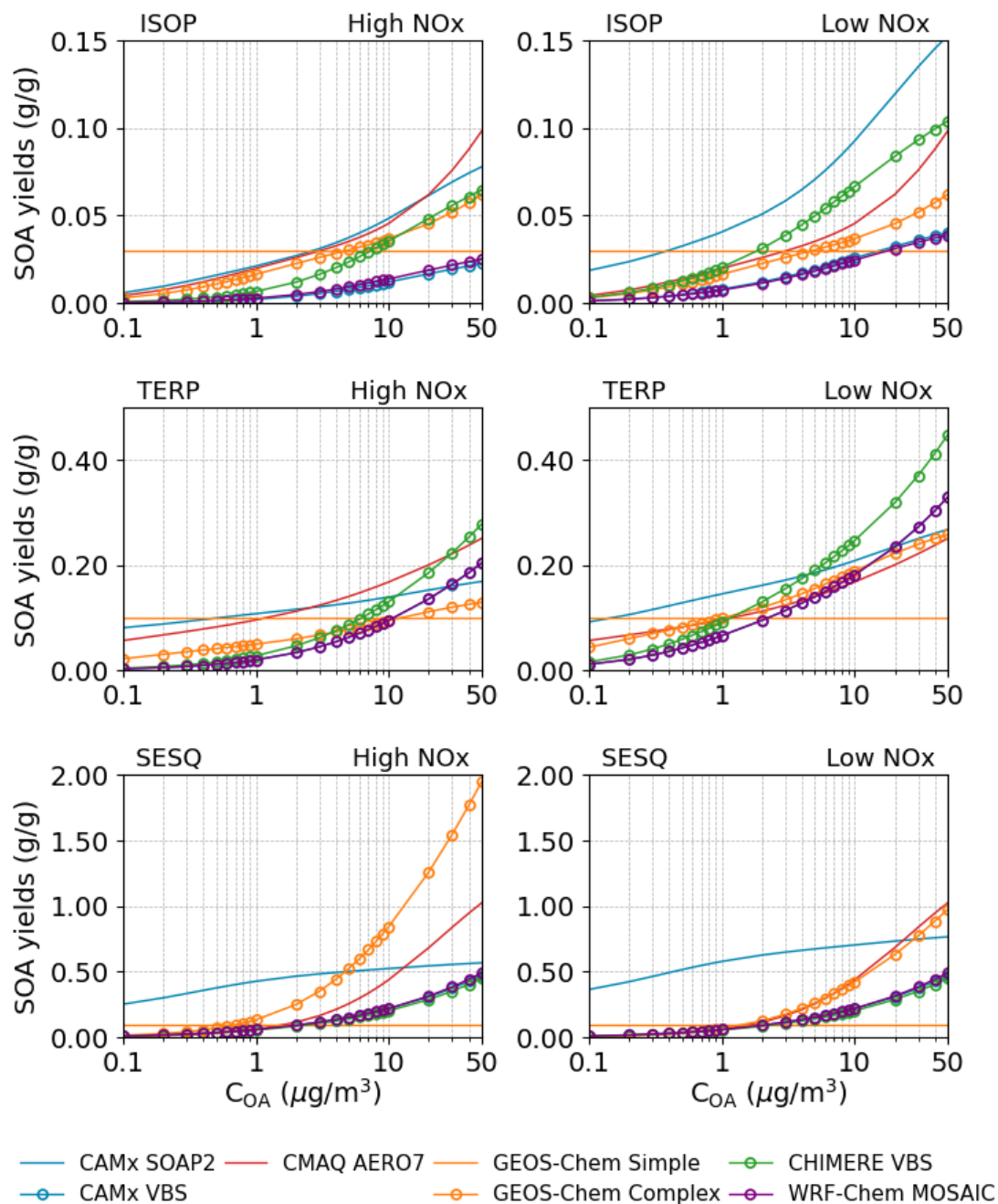
256 ⁷ Multi-model average yield excluding GEOS-Chem Simple for aromatics and IVOC, and excluding CRACMM
 257 for ISOP.

258 ⁸ Ratio of maximum to minimum yield.

259 3.1.2 Non-aged SOA yields from biogenic VOC

260 Figure 4 shows how the non-aged SOA mass yields depend on C_{OA} for three biogenic VOC
261 (BVOC), namely isoprene (ISOP), monoterpenes (TERP), and sesquiterpenes (SESQ). For
262 isoprene, CMAQ includes heterogeneous SOA formation from IEPOX (Pye et al., 2013),
263 which is outside the scope of this evaluation and thus is not discussed in this study.

264 Overall, the BSOA yield patterns closely resemble those of ASOA. All schemes, except for
265 GEOS-Chem Simple, predict an increase in yields associated with C_{OA} . However, the
266 magnitude of SOA yields varies significantly across schemes, ranging from 1.8 to 8.4 under
267 high NO_x conditions and 2.5 to 7.0 under low NO_x conditions. Additionally, model
268 predictions regarding the influence of NO_x on BSOA yields are inconsistent, with some
269 indicating an increase, others a decrease, and some showing no effect. For instance, SOA
270 yields from ISOP under high NO_x conditions, as simulated by two CAMx schemes,
271 WRF-Chem MOSAIC, and CHIMERE VBS, are approximately half of those under low NO_x
272 conditions. In contrast, CMAQ AERO7 and GEOS-Chem schemes suggest that SOA yields
273 are independent of NO_x levels. Regarding TERP-derived SOA, all schemes, except for
274 CMAQ AERO7 and GEOS-Chem Simple, predict more than 50% higher yields under low
275 NO_x conditions compared to high NO_x conditions. The latter two schemes show no
276 difference between NO_x regimes. For SESQ, four models (CAMx VBS, CMAQ AERO7,
277 CHIMERE VBS, and WRF-Chem MOSAIC) predict no distinction in SOA yields between
278 high and low NO_x conditions. Conversely, CAMx SOAP2 suggests higher yields under low
279 NO_x conditions, whereas the GEOS-Chem Complex scheme predicts the opposite.



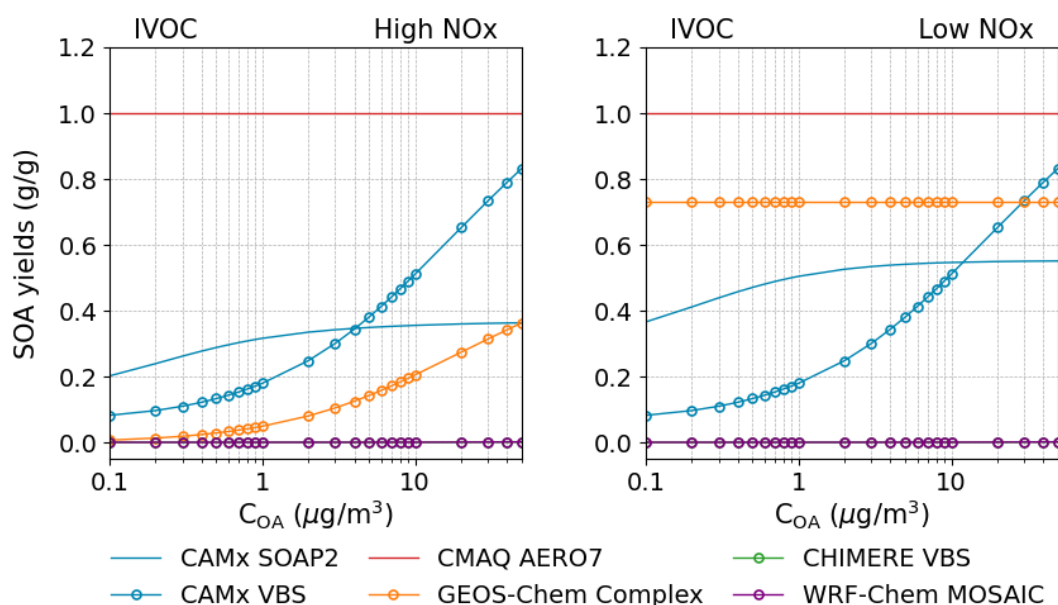
280

281 **Figure 4** Comparison of the non-aged SOA yields (g/g) as functions of C_{OA} for three
 282 biogenic VOC among different schemes (CMAQ CRACMM not included). SOA yields are
 283 calculated at 298 K. Note that y-axis scales vary by precursor to highlight scheme
 284 discrepancies across different yield magnitudes.

285 3.1.3 Non-aged SOA yields from intermediate volatility organic compounds (IVOC)

286 IVOC emissions make important contributions to ASOA formation (Zhao et al., 2016; Ma et
 287 al., 2016; Zhao et al., 2014). The SOA yields from IVOC, referred to as IV-SOA, predicted
 288 by each scheme are shown in Figure 5. The GEOS-Chem Simple scheme is omitted since it

289 does not explicitly account for IVOC. Additionally, the results for CMAQ CRACMM are
 290 discussed separately in Section 4.2.3, due to its distinct treatment of several IVOC types.
 291 SOA yields from IVOC in the CAMx VBS scheme shows a strong positive dependence on
 292 C_{OA} whereas CAMx SOAP2 and GEOS-Chem Complex exhibit much weaker responses.
 293 Constant SOA yields of 1.0 g/g are set in CMAQ AERO7, regardless of NO_x levels,
 294 surpassing the values predicted by other schemes. SOA formation from IVOC in CHIMERE
 295 VBS and WRF-Chem MOSAIC is treated as multi-generational oxidation (R13-R18 in
 296 Supplementary Information), resulting in extremely low non-aged SOA yields (<0.001 g/g).



297
 298 **Figure 5** Comparison of the non-aged SOA yields (g/g) as functions of C_{OA} for IVOC
 299 among different schemes (CMAQ CRACMM and GEOS-Chem Simple not included). SOA
 300 yields are calculated at 298 K.

301 3.2 Comparison of SOA aging

302 Among the eight schemes we evaluated, the CAMx SOAP2, GEOS-Chem Simple, and
 303 GEOS-Chem Complex schemes do not incorporate explicit SOA aging processes. However,
 304 the SOAP2 yields are derived from a VBS parameterization that includes aging (Hodzic et al.,
 305 2016) and may therefore be considered pre-aged (Emery et al., 2024). The remaining
 306 schemes account for SOA aging using one or more of three mechanisms: gas-phase
 307 OH-oxidation, condensed-phase oligomerization, and condensed-phase hydrolysis. Gas-phase
 308 OH-oxidation aging is typically parameterized as functionalization reactions that generate

309 less volatile products (e.g. Figure 2b) and/or fragmentation reactions that produce more
310 volatile products (e.g. Figure 2c). This mechanism is adopted in CAMx VBS (for AVOC and
311 IVOCs only), CMAQ CRACMM, WRF-Chem MOSAIC and CHIMERE VBS, with
312 implementation being specific to each scheme. Condensed-phase oligomerization aging (e.g.
313 Figure 2d) is characterized as a first-order particle-phase reaction, usually assuming a lifetime
314 of 30 hr, leading to non-volatile product formation independent of oxidant concentrations.
315 CMAQ AERO7 applies this process for SOA formed from all precursors except
316 monoterpenes. For SOA derived from NO₃ oxidation of monoterpenes, AERO7 instead
317 applies condensed-phase hydrolysis, yielding non-volatile products with a lifetime of ~3 hr.
318 To compare the aging effects on SOA yields across different schemes, we assumed a 24-hour
319 exposure to an OH concentration of 3×10^6 molecules/cm³ (equivalent to 2.6×10^{11}
320 molecules·s·cm⁻³) for the OH-oxidation aging process or a 24-hour of condensed-phase
321 oligomerization/hydrolysis when calculating the aged SOA yields (details presented below).
322 Table 3 summarizes the aged SOA yields (when applicable) at 298 K with a C_{OA} of 10 µg/m³
323 as simulated by each scheme. Figure 6 and Figure 7 further compare the non-aged and aged
324 SOA yields for each scheme and SOA precursor, while Figure 8 separately illustrates the
325 aging effects on IVOC-derived SOA across different schemes.

326 3.2.1 Aging in CAMx VBS

327 The CAMx VBS scheme incorporates step-wise gas-phase OH-oxidation aging for AVOC
328 and IVOC without accounting for fragmentation processes (Figure 2b). The calculation of
329 aged SOA yields follows Eq. 3 to Eq. 5, using a k_{OH} value of 2×10^{-11} cm³ molecule⁻¹ s⁻¹ and
330 an OH concentration of 3×10^6 molecules cm⁻³. Figure 7a-b illustrates how SOA yields
331 change as a function of accumulated OH exposure under high and low NO_x conditions for
332 different precursors. In the CAMx VBS scheme, SOA yields increase with OH exposure
333 though the rate of aging slows as the OH exposure increases. With a 24-hour period
334 (corresponding to an OH exposure of 2.6×10^{11} molecules·s·cm⁻³), SOA yields from aromatics
335 increase by a factor of 5-6 under high NO_x conditions and 3-5 under low NO_x conditions
336 compared to their non-aged yields. For IVOC, aged SOA yields increase by 125% relative to

337 the non-aged yields (Figure 8b). These findings highlight the significant influence of aging
 338 processes implemented in the CAMx VBS scheme.

339

340 **Table 3** Aged SOA yields (g/g) for different precursors across schemes at 298 K and C_{OA} of
 341 $10 \mu\text{g}/\text{m}^3$. Shaded values indicate no aging effect (i.e. identical to values in Table 2).

| Precursor- NO _x case | CM _x ¹ SP2 | CM _x VBS | CMQ AE7 | CMQ CRM | G-C Spl | G-C Cpx | CMR VBS | W-C MOS | Avg ⁷ | Max/ Min ⁸ |
|------------------------------------|-------------------------------------|------------------------|------------|------------|------------|------------|------------|------------|------------------|--------------------------|
| BENZ ² -high | 0.51 | 0.80 | 0.22 | 0.23 | / | 0.14 | 0.79 | 0.18 | 0.41 | 5.6 |
| BENZ-low | 0.40 | 1.07 | 0.37 | 0.67 | / | 0.37 | 1.11 | 0.20 | 0.60 | 5.6 |
| TOL ³ -high | 0.48 | 1.30 | 0.12 | 0.11 | / | 0.08 | 0.79 | 0.18 | 0.44 | 15.7 |
| TOL-low | 0.93 | 1.33 | 0.30 | 0.50 | / | 0.30 | 1.11 | 0.20 | 0.67 | 6.7 |
| XYL ⁴ -high | 0.11 | 0.83 | 0.07 | 0.09 | / | 0.05 | 0.66 | 0.18 | 0.29 | 16.9 |
| XYL-low | 0.74 | 1.14 | 0.36 | 0.51 | / | 0.36 | 0.98 | 0.20 | 0.61 | 5.7 |
| IVOC ⁵ high | 0.36 | 1.15 | 1.00 | 0.31 | / | 0.20 | 0.02 | 1.20 | 0.60 | 73.7 |
| IVOC-low | 0.55 | 1.15 | 1.00 | 0.53 | / | 0.73 | 0.02 | 1.20 | 0.74 | 73.7 |
| ISOP-high | 0.05 | 0.01 | 0.06 | / | 0.03 | 0.04 | 0.08 | 0.01 | 0.04 | 6.8 |
| ISOP-low | 0.09 | 0.03 | 0.06 | / | 0.03 | 0.04 | 0.12 | 0.02 | 0.06 | 5.0 |
| TERP-high | 0.14 | 0.09 | 0.17 | 0.84 | 0.10 | 0.09 | 0.54 | 0.10 | 0.26 | 5.7 |
| TERP-low | 0.21 | 0.18 | 0.17 | 0.20 | 0.10 | 0.19 | 0.80 | 0.18 | 0.25 | 17.5 |
| SESQ ⁶ -high | 0.52 | 0.22 | 0.78 | 0.54 | 0.10 | 0.84 | 0.86 | 0.22 | 0.51 | 8.6 |
| SESQ-low | 0.70 | 0.22 | 0.78 | 1.04 | 0.10 | 0.42 | 0.86 | 0.22 | 0.54 | 10.4 |

342 ¹ Model name abbreviations are CM_x for CAM_x, CMQ for CMAQ, G-C for GEOS-Chem, CMR for
 343 CHIMERE, and W-C for WRF-Chem. Scheme name abbreviations are SP2 for SOAP2, AE7 for AERO7, Spl
 344 for Simple, Cpx for Complex, and MOS for MOSAIC.

345 ² For WRF-Chem and CHIMERE, results for BENZ are based on ARO1.

346 ³ For WRF-Chem and CHIMERE, results for TOL are based on ARO1.

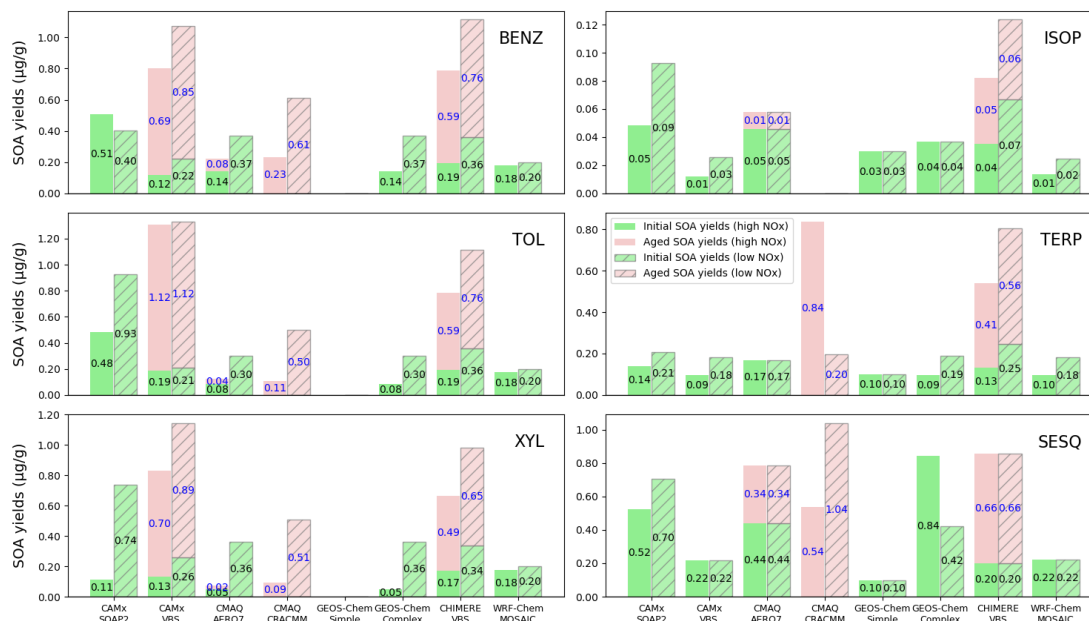
347 ⁴ For WRF-Chem and CHIMERE, results for XYL are based on ARO2. For CMAQ CRACMM, results for
 348 XYL are averages of XYE and XYM.

349 ⁵ For CMAQ CRACMM, IVOC yields are average of alkane and oxygenated IVOCs (see details in Table S17).
 350 For WRF-Chem MOSAIC, IVOC is assumed to have 50% oxygen.

351 ⁶ For CHIMERE, results for SESQ are based on humulene.

352 ⁷ Multi-model average yield excluding GEOS-Chem Simple for aromatics and IVOC, and excluding CRACMM
 353 for ISOP.

354 ⁸ Ratio of maximum to minimum yield.



355

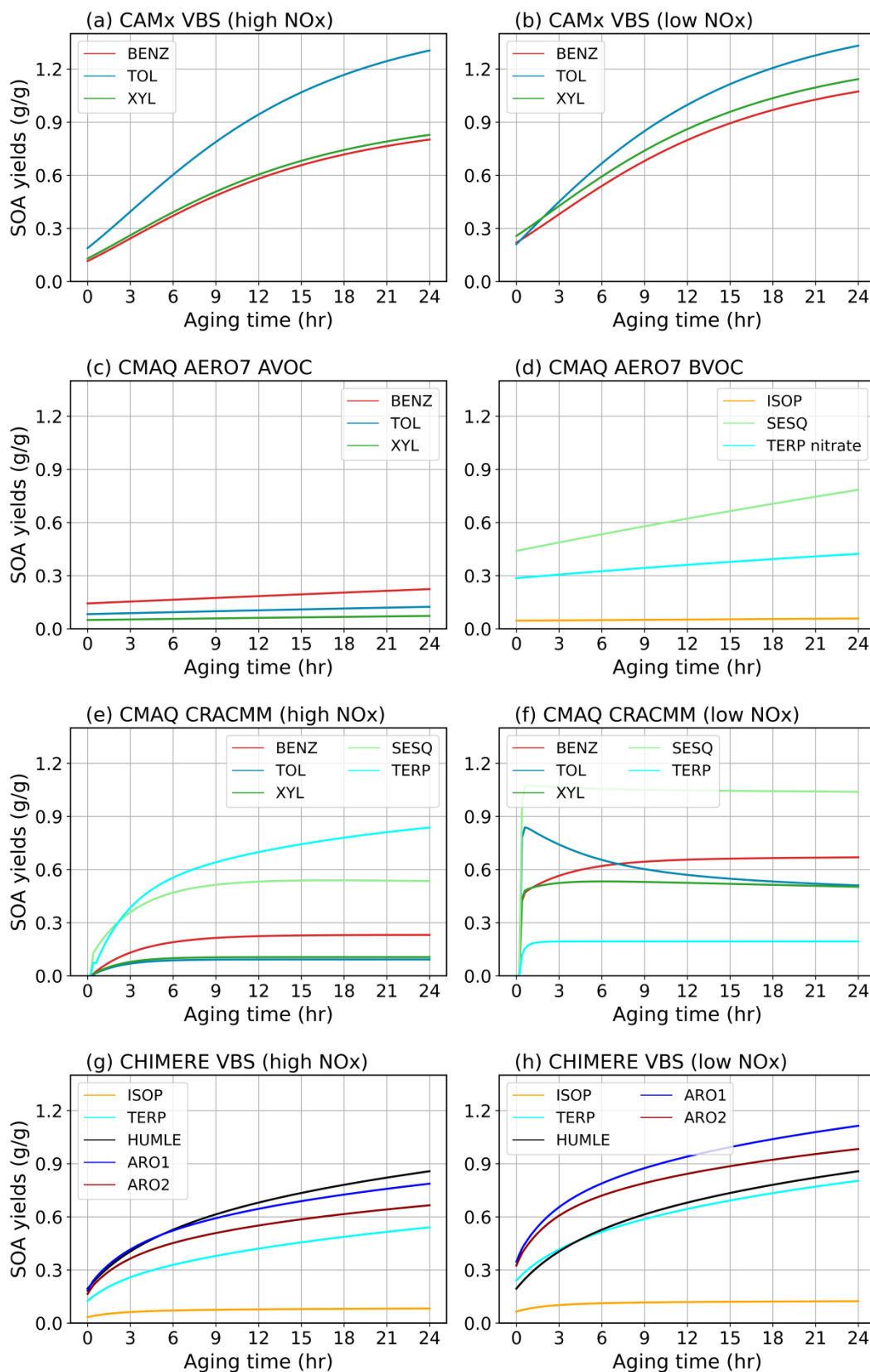
356 **Figure 6** Effect of aging on SOA yields (g/g) for different precursors under high
 357 and low NO_x conditions. Note that y-axis scales vary by precursor to highlight
 358 scheme discrepancies across different yield magnitude.

359 3.2.2 Aging in CMAQ AERO7

360 The SOA aging process in the CMAQ AERO7 scheme involves particle-phase
 361 oligomerization (Figure 2d) and hydrolysis. Oligomerization applies to SOA formed
 362 from ISOP, SESQ, and aromatics (only under high-NO_x conditions) while hydrolysis
 363 affects SOA formed from monoterpenes oxidation by NO₃ radical. The aged SOA
 364 yields resulting from oligomerization and hydrolysis follows Eq. 6 to Eq. 8, with rate
 365 constants $k_{\text{OLIG}} = 9.49 \times 10^{-6} \text{ s}^{-1}$ and $k_{\text{hydro}} = 9.26 \times 10^{-5} \text{ s}^{-1}$. Figure 7b illustrates the
 366 evolution of SOA yields over 24 hours of oligomerization, showing increases of 27%,
 367 79%, and 46%-57% for ISOP, SESQ, and aromatics, respectively. This increase
 368 results from the reduced volatility of SOA due to oligomerization. The hydrolysis
 369 reaction, assuming a shorter lifetime of approximately 3 hr, leads to a 48% increase in
 370 SOA yield from monoterpene-derived organic nitrates over 1 day. Although the
 371 hydrolysis rate is nearly ten times faster than that of oligomerization, the overall yield
 372 increase is moderated because the hydrolysis products have lower molecular weights
 373 than their parent compounds.

374 3.2.3 Aging in CMAQ CRACMM

375 The aging processes in CMAQ CRACMM involve the gas-phase OH-oxidation
376 reactions of secondary oxygenated L/S/IVOCs, leading to both fragmentation and
377 functionalization, and resulting in products with varying volatilities. As illustrated in
378 Figure 7e-f, the impact of aging on SOA yields depends on the precursor and varies
379 between high NO_x and low NO_x conditions. Under high NO_x conditions, SOA yields
380 from all precursors increase substantially during the first 6-8 hours, after which the
381 growth rate becomes negligible (except for TERP, which continues to increase). After
382 24 hours of aging, SOA yields under high NO_x conditions range from 0.093 g/g for
383 XYL to 0.838 g/g for TERP (Table 3). In contrast, under low NO_x conditions, all
384 precursors show a sharp increase in SOA yields within the first 30 mins. Subsequently,
385 SOA yields from XYL begin to decline, gradually reaching a minimum value of
386 approximately 0.511 g/g after 16 hours. On the contrary, BENZ yields continue to
387 increase slightly, peaking around 0.670 g/g. TERP, TOL, and SESQ yields exhibit
388 minimal change after their initial increase. After 24 hours, SOA yields under low NO_x
389 conditions range from 0.195 g/g for TERP to 1.039 g/g for SESQ.



390

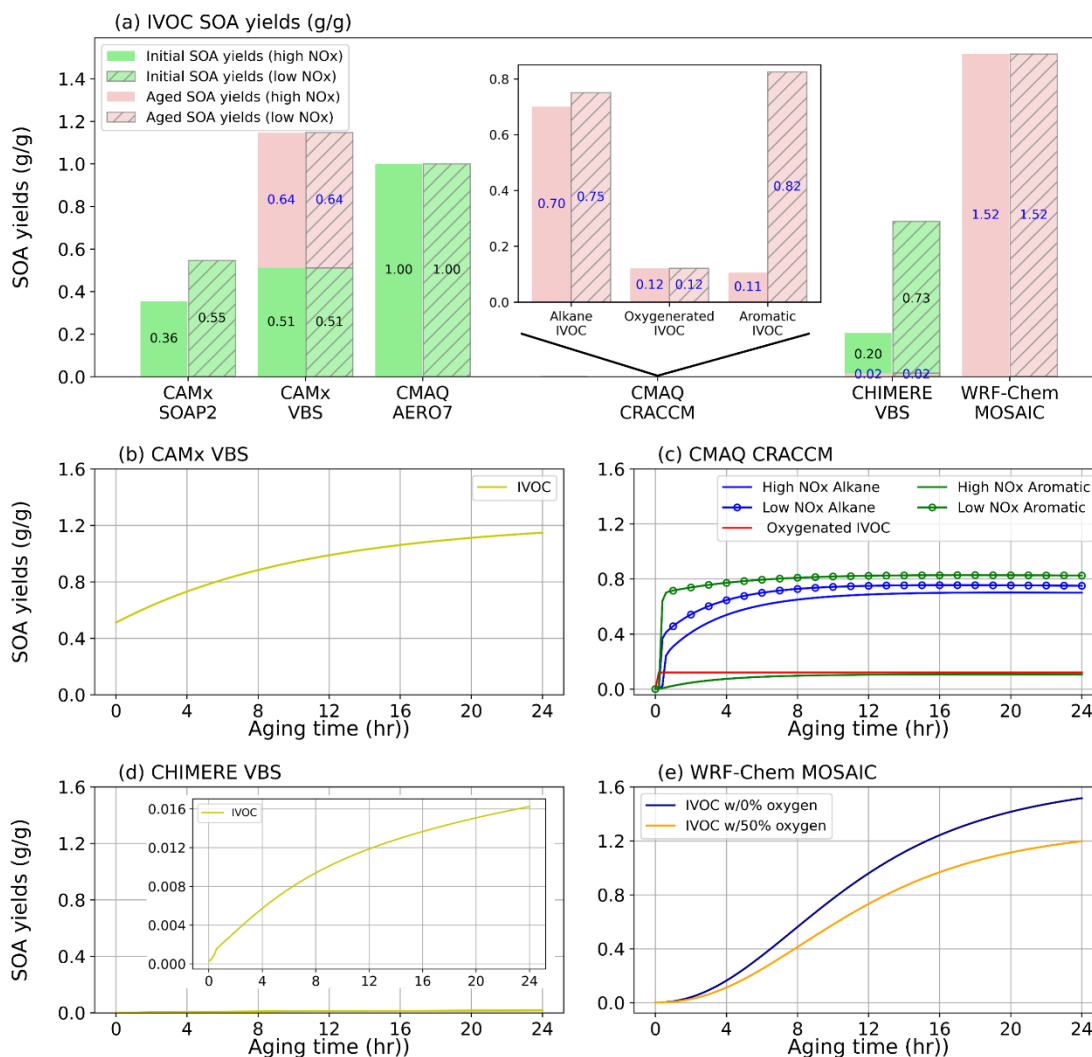
391

392

Figure 7 Effect of aging on SOA yields (g/g) from different precursors as a function of OH exposure or aging time in different schemes. (a-b) CAMx VBS; (c-d) CMAQ

393
394

AERO7; (e-f) CMAQ CRACMM; and (g-h) CHIMERE VBS. The numbers in the brackets indicate the relative change of SOA yields at hour 24 to hour 0.



395

396 **Figure 8** Effect of aging on SOA yields (g/g) for IVOC precursors under high and
397 low NOx conditions for different schemes.

398 Unlike other schemes, the CMAQ CRACMM scheme classifies IVOC into alkanes,
399 aromatics, and oxygenated IVOC based on their functional groups. Emitted
400 oxygenated IVOC do not exhibit aging effects, as their oxidation products are
401 assumed to be non-volatile (Figure 8c). In contrast, SOA yields from alkane and
402 aromatic IVOC increase with the aging time, with the growth rate becoming
403 negligible after approximately 10 hours. SOA yields from oxygenated IVOC (0.121
404 g/g) are independent of NOx conditions. The other two IVOC types show higher SOA
405 yields under low NOx conditions, particularly for aromatic IVOC, where the SOA

406 yields under low NO_x conditions (0.825 g/g) are nearly 8 times that under high NO_x
407 conditions (0.105 g/g).

408 3.2.4 Aging in CHIMERE VBS

409 The CHIMERE VBS scheme accounts for aging through gas-phase functionalization
410 and fragmentation, as well as condensed-phase oligomerization, as shown in
411 Supplementary Information R9 to R12. Figure 7d presents the combined aging effects
412 on SOA over a 24-hour period under this scheme. Among BVOC, the aging effect is
413 more pronounced for TERP and humulenes (HUMULE) than for ISOP. Under high
414 NO_x conditions, the SOA yields from ISOP, TERP, and HUMULE increase by 141%,
415 331%, and 341%, respectively, over one day. In contrast, under low NO_x conditions,
416 the aging effect is generally less significant, except for HUMULE, which exhibits a
417 similar level of aging under both NO_x regimes. Aromatics show substantial increase
418 in SOA yields—over 300% under high NO_x and 200% under low NO_x conditions.

419 Aging of SOA from IVOC results in a dramatic increase in yields—by nearly a factor
420 of 60 within one day, as shown by Figure 8d. However, the absolute SOA yields from
421 IVOC remain low (approximately 0.01 g/g), which is attributed to the non-aged low
422 SOA formation ($\sim 10^{-4}$ g/g) and the dominance of fragmentation at higher oxidation
423 generations. From the third oxidation generation onward, 75% of the condensable
424 gases undergo fragmentation into more volatile products, while only 15% undergo
425 functionalization, as described in Supplementary Information R14.

426 3.2.5 Aging in WRF-Chem MOSAIC

427 The WRF-Chem MOSAIC scheme does not include SOA aging processes for AVOC
428 and BVOC. SOA formation from IVOC is parameterized as a stepwise gas-phase
429 OH-oxidation process. For the non-oxygen component of condensable gases, a 15%
430 mass gain is assumed for each generation (as per Supplementary Information R15 and
431 R16). Meanwhile, the oxygenated component shifts to lower volatility bins without
432 mass gain (as per Supplementary Information R17 and R18). The scheme does not
433 consider fragmentation or condensed-phase oligomerization. Figure 8e illustrates
434 aging effects under two scenarios: IVOC with hydrocarbon-like characteristics (0%

435 oxygen by mass at $t=0$, representing of diesel emissions) and IVOC with 50% oxygen
436 by mass (representing of biomass burning emissions). In both cases, the
437 non-fragmenting stepwise aging process in WRF-Chem results in substantial increases
438 in SOA yields. At an OH exposure of 2.6×10^{11} molecule \cdot s \cdot cm $^{-3}$ (i.e. a 24-hour period),
439 SOA formed from hydrocarbon-like IVOC exceeds 1 g/g, despite an initially
440 negligible yield.

441 **3.3 NO_x effects on SOA yields**

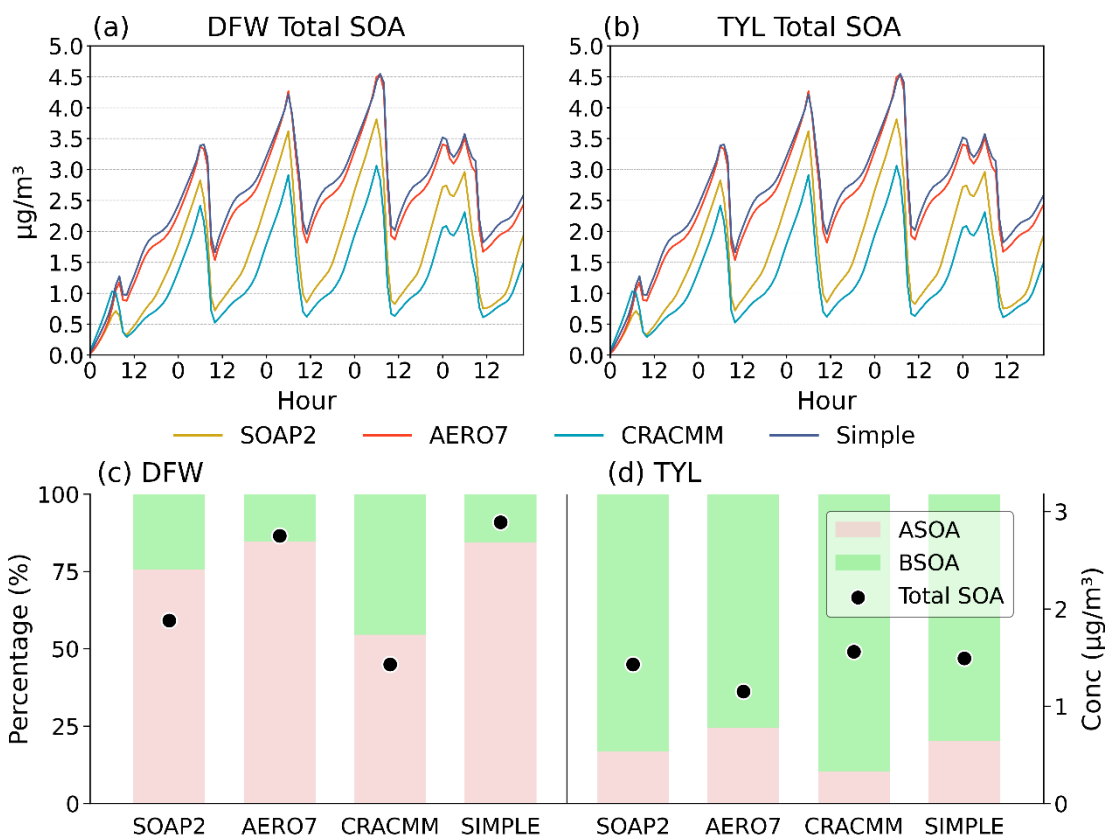
442 Evaluating SOA yields for seven precursor types across eight modeling schemes
443 results in 56 potential characterizations of how NO_x levels influence SOA formation.
444 Table S18 and S19 present the ratios of non-aged and aged SOA yields under high and
445 low NO_x conditions. For non-aged SOA yields, 11 of the 56 cases are missing and 14
446 cases are designed to exhibit no NO_x dependence, leaving 31 meaningful comparisons.
447 Among these, 29 cases show lower SOA yields under high NO_x conditions. For aged
448 SOA yields, 5 cases are missing and 14 are designed with no NO_x effect, leaving 37
449 meaningful comparisons, of which 34 also show lower SOA yields under high NO_x
450 conditions. These results indicate a general trend of higher SOA yields under low
451 NO_x conditions, although a few exceptions are observed. In some cases, the NO_x
452 effect is reversed—that is, SOA yields are higher under high NO_x conditions than
453 under low NO_x conditions. This is seen for BENZ in the CAMx SOAP2 scheme,
454 TERP in CMAQ CRACMM, and SESQ in the GEOS-Chem Complex scheme. The
455 NO_x effect on terpene-derived SOA in CRACMM is particularly noteworthy: the
456 model predicts an eightfold increase in SOA yields under high NO_x conditions
457 compared to low NO_x. This is significant given that terpenes are key SOA precursors
458 in many forested regions, such as the Eastern U.S., where anthropogenic NO_x
459 emissions may change due to ongoing urban development (which could increase NO_x
460 levels) or the implementation of emission control technologies (which may reduce
461 them). Experimental studies, including those by Sarrafzadeh et al. (2016) and Wildt et
462 al. (2014), have consistently found that terpene-derived SOA yields are higher under
463 low NO_x conditions, a result that aligns with most of the evaluated schemes but

464 contrasts with the predictions made by CRACMM.

465 **3.4 SOA variations in box model simulations**

466 The box model simulations reveal significant discrepancies in predicted SOA
467 concentration and composition among the selected schemes at both the urban (DFW)
468 and rural (TYL) locations (Figure 9). The total SOA concentrations can vary by a
469 factor of 2–3 between schemes even under identical meteorological and emission
470 inputs. Overall, SOA concentrations are higher at DFW than at TYL. At both locations,
471 all schemes exhibit a consistent diurnal profile characterized by SOA accumulation
472 throughout the day and night, followed by a sharp decline in the early morning
473 (beginning around 06:00 LST) caused by expansion of the planetary boundary layer
474 (PBL). At DFW, the temporal trends are similar across the four schemes; however, the
475 magnitude varies, with Simple and AERO7 predicting the highest concentrations,
476 while CRACMM predicts the lowest. At TYL, the inter-model spread is narrower than
477 at DFW. Notable differences in diurnal dominance emerge: SOAP2 and CRACMM
478 predict the highest concentrations overnight—a pattern distinct from DFW—while
479 Simple and CRACMM produce the highest values during daytime hours. Figure 9c-d
480 shows the maximum and minimum average SOA concentrations. At DFW, Simple and
481 CRACMM predict the highest and lowest total SOA concentrations, respectively.
482 Conversely, at TYL, CRACMM predicts the highest average concentration, while
483 AERO7 predicts the lowest.

484



485

486 **Figure 9** Diurnal profiles of total SOA ($\mu\text{g}/\text{m}^3$) from the 5-day box model base
 487 simulations at (a) DFW and (b) TYL. Average SOA concentrations ($\mu\text{g}/\text{m}^3$)
 488 averaged over days 2 through 5 of base model simulations for each SOA scheme
 489 (circles) and average contributions of ASOA and BSOA (bars)

490 Response surface plots for 24-hour average SOA concentrations derived from the
 491 matrix of simulations with varied anthropogenic NO_x and VOC emissions are
 492 presented in Figure S4-S5. At DFW, total SOA concentrations generally decrease as
 493 anthropogenic NO_x emissions increase relative to the base case (scaling factors 2–9)
 494 for all schemes, with the notable exception of CRACMM. CRACMM predicts
 495 negligible changes or a slight increase in SOA as NO_x rises from low to mid scaling
 496 factors and a decrease is observed only when NO_x emissions are increased by about a
 497 factor of 7 or greater. CRACMM also predicts the lowest SOA concentrations across
 498 all scaling factors. AERO7 and SIMPLE are very similar in both response surface
 499 shape and magnitude. For each scheme, SOA concentrations decrease as the
 500 anthropogenic VOC emissions decrease. At TYL, the response surfaces for AERO7,
 501 Simple, and SOAP3 are similar, with SOA concentrations remaining relatively

502 constant at NO_x scaling factors greater than 1. In contrast, CRACMM demonstrates a
503 much stronger response, with SOA mass increasing concurrently with NO_x emissions.
504 At this biogenic-dominated site, SOA concentrations in all schemes are minimally
505 sensitive to variations in anthropogenic VOC emissions.

506 Understanding how SOA responds to NO_x reductions is critical for near-term air
507 quality planning, as many regulatory strategies (e.g., cleaner vehicles, energy
508 transition) produce substantial NO_x emissions abatement (Crippa et al. 2016; EPA et
509 al. 2017; Li et al. 2024). Table 4 summarizes the impact of a 50% reduction in NO_x
510 emissions on total SOA, ASOA, and BSOA. In all schemes, reducing NO_x leads to
511 increased ASOA concentrations, with the most pronounced increase predicted by
512 SOAP2. SIMPLE predicts the smallest increase in ASOA at DFW, while CRACMM
513 predicts the smallest increase at TYL. At DFW, this NO_x reduction also drives an
514 increase in BSOA concentrations across most schemes, with the notable exception of
515 CRACMM. Consistent with the ASOA results, SOAP2 predicts the largest increase in
516 BSOA. The distinct behavior in CRACMM is driven by its monoterpene SOA
517 parameterization; contrary to other schemes and experimental evidence (Lane et al.
518 2008; Sarrafzadeh et al. 2016, Zhao et al. 2018), CRACMM predicts decreasing
519 yields under lower NO_x conditions. Consequently, the substantial reduction in BSOA
520 predicted by CRACMM at DFW results in a net decrease in total SOA, a trend
521 opposite to that observed in the other schemes. At TYL, all schemes predict a
522 decrease in both BSOA and total SOA, with the most significant reductions observed
523 in the CRACMM simulation. The dominance of biogenic emissions at TYL compared
524 to DFW is reflected in the significantly higher BSOA concentrations. The differing
525 SOA responses to NO_x reduction between the two sites are attributable to the distinct
526 biogenic emission regimes producing different VOC/NO_x emission ratios.

527 **Table 4** Average concentrations ($\mu\text{g}/\text{m}^3$) of anthropogenic SOA (ASOA) and
 528 biogenic SOA (BSOA) over days 2 through 5 for the base and reduced NO_x model
 529 simulations. Shading indicates a decrease in SOA concentrations in the reduced NO_x
 530 model runs compared to the base runs.

| Location | Species | SOAP2 | | | AERO7 | | |
|----------|-----------|--------|---------------------|----------|--------|---------------------|----------|
| | | Base | 50% NO _x | Diff (%) | Base | 50% NO _x | Diff (%) |
| DFW | ASOA | 1.34 | 1.48 | 9.60% | 2.34 | 2.38 | 1.90% |
| | BSOA | 0.42 | 0.48 | 12.20% | 0.41 | 0.42 | 0.40% |
| | Total SOA | 1.76 | 1.96 | 10.30% | 2.75 | 2.8 | 1.60% |
| TYL | ASOA | 0.24 | 0.25 | 4.40% | 0.28 | 0.31 | 9.90% |
| | BSOA | 1.19 | 1.14 | -4.10% | 0.87 | 0.82 | -6.20% |
| | Total SOA | 1.43 | 1.4 | -2.50% | 1.16 | 1.14 | -1.80% |
| Location | Species | CRACMM | | | Simple | | |
| | | Base | 50% NO _x | Diff (%) | Base | 50% NO _x | Diff (%) |
| DFW | ASOA | 0.78 | 0.81 | 3.50% | 2.44 | 2.45 | 0.60% |
| | BSOA | 0.65 | 0.59 | -10.70% | 0.45 | 0.46 | 2.40% |
| | Total SOA | 1.43 | 1.4 | -2.50% | 2.88 | 2.91 | 0.90% |
| TYL | ASOA | 0.16 | 0.17 | 1.00% | 0.3 | 0.32 | 8.50% |
| | BSOA | 1.4 | 1.24 | -12.60% | 1.19 | 1.14 | -4.40% |
| | Total SOA | 1.56 | 1.41 | -11.00% | 1.49 | 1.46 | -1.50% |

531 **4. Implications**

532 **SOA schemes implemented in CTMs are diverse, making quantitative**
 533 **comparisons inherently challenging.** CTMs employ diverse approaches to simulate
 534 SOA, from simple schemes that treat SOA_{pre} as non-volatile to more complex VBS
 535 schemes that utilize multiple basis sets to represent different types of precursors.
 536 Variability in how SOA aging is treated further adds to the overall diversity across
 537 schemes. In our view, such diversity is valuable from a research perspective, given
 538 that the underlying processes driving SOA formation remain uncertain and, in many
 539 cases, poorly characterized. The variation in SOA yields across different schemes
 540 reflects the extent of these uncertainties. The differences in scheme formulation,
 541 coupled with the large numbers of parameters employed in some schemes, pose
 542 practical challenges for applying multiple schemes to standardized scenarios.
 543 Addressing these challenges may require innovative approaches. Nonetheless,

544 comparisons under standardized conditions are essential for achieving meaningful
545 quantitative inter-comparisons. Evaluating SOA yields under standard conditions and
546 plotting SOA yield curves (i.e., yield vs. C_{OA}) are effective strategies for identifying
547 similarities and differences among schemes. However, it is important to note that the
548 results presented here may not fully capture the ranges of conditions encountered in
549 three-dimensional atmospheric simulations.

550 **Non-aged SOA yields vary substantially across schemes and while many schemes**
551 **consider SOA aging, the aging effects vary.** Evaluating seven precursor types under
552 both high and low NO_x conditions yields 14 distinct comparisons. Across these
553 comparisons, the ratio of maximum to minimum non-aged yields (max/min) ranges
554 from 1.8 to >1000 with a median max/min of 4.2 (Table 2). Among the eight schemes
555 examined, three (CAMx SOAP2, GEOS-Chem schemes) do not include explicit SOA
556 aging processes. Four schemes account for aging in a subset of precursor types and/or
557 NO_x -conditions, while only one (CMAQ CRACMM) includes aging for all
558 precursors. Aging mechanisms considered by these schemes include gas-phase
559 OH-oxidation of evaporated SOA, particle-phase oligomerization, hydrolysis, and
560 photolysis. The impacts of aging on SOA yields vary by scheme and precursor (Table
561 S20): in 67 of the 98 evaluated cases (defined as one scheme/precursor/ NO_x -condition
562 combination, CRACMM excluded), aging has no effect; in 31 cases, it increases SOA
563 yields. Considering the aging effects, the ratio of max/min aged yields ranges from
564 5.0 to > 70, with a median value of 8.3 (Table 3). The relative rankings of precursors
565 by their initial/aged SOA yields differ across schemes (Table S21 and Table S22),
566 indicating that different aging schemes can lead to divergent conclusions regarding
567 the relative importance of specific SOA precursors—a consideration with potential
568 implications for policy guidance. For instance, discrepancies in yields lead to different
569 precursor rankings (e.g., the relative importance of aromatics vs. IVOCs). A model
570 that underpredicts the SOA potential of IVOC emissions might disproportionately

571 focus policy strategies on traditional VOCs (e.g., from petroleum-based solvents) and
572 potentially lead to ineffective widespread controls that miss the critical contribution of
573 IVOCs.

574 SOA aging remains an area in need of improved representation, with careful attention
575 required to ensure consistent underlying assumptions. Notably, only the two CAMx
576 schemes incorporate condensed-phase SOA photolysis, despite growing evidence that
577 both anthropogenic and biogenic SOA can undergo substantial photolytic depletion
578 (Hodzic et al., 2016; Baboomian et al., 2020), although a portion of SOA appears
579 recalcitrant to such degradation (O'Brien and Kroll, 2019).

580 **Large uncertainty exists for IVOC SOA yields.** The SOA yields from IVOCs show
581 wider variation (from negligible to 1.0 g/g) than for other anthropogenic precursors
582 (Table 2 and Table 3), partly due to different assumptions across schemes. For
583 example, schemes such as WRF-Chem MOSAIC and CHIMERE VBS predict very
584 low non-aged yields from IVOC, based on the assumption that several generations of
585 oxidation are required before forming condensable products. Even after one day of
586 aging, IVOC SOA yields remain highly variable, ranging from 0.02 to 1.20 g/g.
587 Although IVOC are generally classified based on volatility, factors such as high
588 molecular weight or the presence of polar functional groups can shift compounds into
589 the IVOC volatility range (Pankow and Asher, 2008). As a result, volatility and SOA
590 yield are not necessarily well correlated (Donahue et al., 2011). Improving model
591 representations of IVOC-derived SOA yields will require more detailed differentiation
592 of IVOC emissions into multiple subtypes, as illustrated by the CRACMM scheme
593 (Pye et al. 2023). A unified classification or “lumping” scheme for IVOC would be
594 particularly advantageous, allowing multiple models to utilize a common emissions
595 framework and enabling more direct comparisons of IVOC SOA yields. Improving
596 the representation of oxygenated VOCs with reduced volatility—such as glycols and
597 glycol ethers—within gas-phase chemical mechanisms can also support improved

598 differentiation of IVOC-related SOA formation (Yarwood and Tuite, 2024; Yu et al.,
599 2024). More generally, a yield-based lumping approach for IVOCs (e.g., categorizing
600 them into low, medium, or high yield classes) may be more practical to implement
601 than strictly chemically-based schemes.

602 **Determining experimental SOA yields also presents significant challenges.**

603 Laboratory experiments play a crucial role in guiding SOA model development and
604 constraining key model parameters, particularly yields. However, these experiments
605 are subject to operational and design limitations, including the need to account for
606 chamber wall effects (Zhang et al., 2014) and to achieve atmospherically relevant
607 concentration ranges (Peng et al., 2022; Kenagy et al., 2024). The role of autoxidation
608 reactions in SOA formation further complicates the design of atmospherically relevant
609 experiments, as discussed in detail by Kenagy et al. (2024). For instance, studying a
610 reaction mechanism that includes RO₂ radical autoxidation at a rate of 0.1 s⁻¹ requires
611 that the effective rates of competing bimolecular reactions, particularly RO₂ + NO, be
612 reduced to 0.1 s⁻¹ or lower. This necessitates NO mixing ratios below approximately 5
613 ppb, which are now typical of photochemically active urban environments such as Los
614 Angeles (Praske et al., 2018). Many SOA chamber experiments designed to
615 investigate high NO_x conditions exceed 5 ppb NO, thereby preventing autoxidation.
616 Some chamber experiments, such as those by Sarrafzadeh et al. (2016), have been
617 specifically designed to achieve atmospherically relevant NO (and other radicals)
618 concentrations, making their results particularly valuable for SOA model development.
619 In contrast, oxidation flow reactors face greater challenges (Peng et al., 2019) than
620 chamber experiments in studying SOA formation due to their amplification of radical
621 concentrations, which significantly shortens RO₂ lifetime and effectively suppresses
622 autoxidation reactions. Wennberg (2023) has suggested shifting from the conventional
623 terminology of high/low NO_x to high/low NO to emphasize the critical role of NO
624 concentration in determining RO₂ radical fate.

625 **5. Conclusions**

626 In this study, we compared SOA formation by eight schemes implemented in five
627 widely used CTMs. For each SOA scheme, we quantified the non-aged SOA mass
628 yields under standardized conditions ($T=298\text{ K}$ and $C_{\text{OA}}=10\text{ }\mu\text{g/m}^3$), showed how the
629 non-aged yield varies with C_{OA} , and quantified how one day of simulated atmospheric
630 aging changed the non-aged yield. We calculated yields for 7 SOA precursor types (4
631 anthropogenic and 3 biogenic) under both high and low NO_x conditions.

632 The lack of consistency across eight current SOA schemes reviewed here reveals a
633 lack of consensus within the air quality modelling community, notwithstanding
634 substantial efforts to greatly expand the scientific knowledge base related to SOA
635 formation over recent decades. Evaluating SOA schemes using ambient measurements
636 is unlikely to produce consensus because large uncertainties in the SOA schemes are
637 confounded with large uncertainties in precursor emission estimates. In our view,
638 there is no objective basis for preferring one SOA scheme over another considering
639 the high degree of uncertainty presented here. Complex SOA schemes may be
640 valuable to research for investigating linkages between precursors and SOA, but
641 conversely, complexity may be a hindrance to the work of air quality planning
642 because it adds to computational burdens and makes the science more difficult to
643 comprehend and communicate. Notably, very simple SOA schemes have performed as
644 well or better than complex schemes in their ability to simulate ambient OA
645 measurements when driven by ambient precursor measurements (Hodzic and Jimenez,
646 2011; Pai et al., 2020). Complex schemes can introduce responses to conditions, such
647 as NO_x concentration, that may be unexpected and should be overtly evaluated if they
648 have policy relevance, such as the NO_x effect on SOA yield from BVOC. Simple
649 schemes with well-characterized SOA yields and responses can have an important
650 place in air quality modelling to support decision making which includes studies that
651 value the health-burdens of air pollution as well as traditional emissions management

652 planning.

653 In addition, a majority of the eight schemes reviewed here are based on the VBS
654 approach and we expect that sampling a larger number of model schemes would not
655 change this finding. VBS schemes have practical advantages because experimental
656 studies frequently summarize their data (e.g., SOA yields, POA volatility) in a VBS
657 frame which makes for direct translation of these data into a VBS model scheme.
658 However, VBS data can be translated into a different frame (e.g., a two-product
659 scheme) for SOA formation or for representing the partial evaporation of POA
660 emissions, as illustrated by Huang et al. (2024). Therefore, scheme developers can
661 consider using non VBS-based approaches to gain advantages of simplicity and
662 efficiency. The findings summarized above underscore the importance of
663 understanding the limitations of available SOA schemes when applied to air quality
664 management and policy development. The choice of model/scheme can significantly
665 influence the predicted SOA concentrations and their evolution over time, which in
666 turn affects air quality forecasts, assessments and regulations.

667 **DATA AVAILABILITY**

668 The source data for the figures, including an example of the offline calculation (i.e.
669 CMAQ AERO7), are available at Zenodo (<https://doi.org/10.5281/zenodo.16757660>).
670 Calculation data for other species and schemes are available from the corresponding
671 authors upon request.

672 **AUTHOR CONTRIBUTIONS**

673 G.Y. and L.H. designed the research. L.H. performed the data collection, yields
674 calculation, and data analysis. K.T. performed the box model calculation. L.H. K. T.,
675 and G.Y. wrote the manuscript. B. C., Z. W., K.T., P.V., and L.L. contributed to data
676 analysis and revision of the manuscript. All authors contributed to the manuscript
677 preparation and discussions.

678

679 **ACKNOWLEDGMENTS**

680 This work is supported by the Shanghai Technical Service Center of Science and
681 Engineering Computing, Shanghai University. This study was financially supported

682 by the National Natural Science Foundation of China (Grant No. 42375103, 42375102)
683 and Electric Power Research Institute (EPRI), Palo Alto, California.

684

685 **COMPETING INTERESTS**

686 The authors declare no competing interests.

687

688 **REFERENCES**

689 Appel, K. W., Bash, J. O., Fahey, K. M., Foley, K. M., Gilliam, R. C., Hogrefe, C., ...
690 & Wong, D. C. (2021). The Community Multiscale Air Quality (CMAQ)
691 model versions 5.3 and 5.3. 1: system updates and evaluation. *Geoscientific*
692 *Model Development*, 14(5), 2867-2897.

693 Baboomian, V.J., Gu, Y. and Nizkorodov, S.A., 2020. Photodegradation of secondary
694 organic aerosols by long-term exposure to solar actinic radiation. *ACS Earth*
695 *and Space Chemistry*, 4(7), pp.1078-1089.

696 Cappa, C. D., & Wilson, K. R. (2012). Multi-generation gas-phase oxidation,
697 equilibrium partitioning, and the formation and evolution of secondary organic
698 aerosol. *Atmospheric Chemistry and Physics*, 12(20), 9505-9528.

699 Chang, X., Zhao, B., Zheng, H., Wang, S., Cai, S., Guo, F., ... & Donahue, N. M.
700 (2022). Full-volatility emission framework corrects missing and
701 underestimated secondary organic aerosol sources. *One Earth*, 5(4), 403-412.

702 Chen, Q., Miao, R., Geng, G., Shrivastava, M., Dao, X., Xu, B., ... & Zhu, T. (2024).
703 Widespread 2013-2020 decreases and reduction challenges of organic aerosol
704 in China. *Nature Communications*, 15(1), 4465.

705 Crippa, M., Janssens-Maenhout, G., Dentener, F., Guizzardi, D., Sindelarova, K.,
706 Muntean, M., et al. (2016). Forty years of improvements in European air
707 quality: Regional policy-industry interactions with global impacts.
708 *Atmospheric Chemistry and Physics*, 16(6), 3825–3841.

709 CHIMERE Users Guide (2023). <https://www.lmd.polytechnique.fr/chimere/>, accessed
710 on Feb. 15th 2024.

711 Couvidat, F., Bessagnet, B., Garcia-Vivanco, M., Real, E., Menut, L., & Colette, A.
712 (2018). Development of an inorganic and organic aerosol model (CHIMERE
713 2017 β v1. 0): Seasonal and spatial evaluation over Europe. *Geoscientific*
714 *Model Development*, 11(1), 165-194.

715 Donahue, N. M., Robinson, A. L., Stanier, C. O., & Pandis, S. N. (2006). Coupled
716 partitioning, dilution, and chemical aging of semivolatile
717 organics. *Environmental science & technology*, 40(8), 2635-2643.

718 Donahue, N. M., Epstein, S. A., Pandis, S. N., & Robinson, A. L. (2011). A
719 two-dimensional volatility basis set: 1. organic-aerosol mixing
720 thermodynamics. *Atmospheric Chemistry and Physics*, 11(7), 3303-3318.

721 Emery, C.A., Baker, K.R., Wilson, G.M. and Yarwood, G. (2024). Comprehensive
722 Air Quality Model With Extensions, v7. 20: Formulation and Evaluation for
723 Ozone and Particulate Matter Over the US. *Geoscientific Model Development
724 Discussions*, 2024, pp.1-48.

725 EPA. (2017). United States environmental protection agency: Overview of the clean
726 air Act and air pollution. <https://www.epa.gov/clean-air-act-overview>,
727 accessed on March 5th, 2026

728 Hodzic, A. and Jimenez, J.L. (2011). Modeling anthropogenically controlled
729 secondary organic aerosols in a megacity: A simplified framework for global
730 and climate models. *Geoscientific Model Development*, 4(4), pp.901-917.

731 Hodzic, A., Jimenez, J. L., Madronich, S., Canagaratna, M. R., DeCarlo, P. F.,
732 Kleinman, L., & Fast, J. (2010). Modeling organic aerosols in a megacity:
733 potential contribution of semi-volatile and intermediate volatility primary
734 organic compounds to secondary organic aerosol formation. *Atmospheric
735 Chemistry and Physics*, 10(12), 5491-5514.

736 Hodzic, A.; Kasibhatla, P. S.; Jo, D. S.; Cappa, C. D.; Jimenez, J. L.; Madronich, S.;
737 Park, R. J. Rethinking the global secondary organic aerosol (SOA) budget:
738 stronger production, faster removal, shorter lifetime. *Atmos. Chem. Phys.*
739 2016, 16, 7917–7941.

740 Huang, L., Liu, H., Yarwood, G., Wilson, G., Tao, J., Han, Z., ... & Li, L. (2023).
741 Modeling of secondary organic aerosols (SOA) based on two commonly used
742 air quality models in China: Consistent S/IVOCs contribution but large
743 differences in SOA aging. *Science of The Total Environment*, 903, 166162.

744 Huang, L., Zi'ang Wu, H. L., Yarwood, G., Huang, D., Wilson, G., Chen, H., ... & Li,
745 L. (2024). An improved framework for efficiently modeling organic aerosol
746 (OA) considering primary OA evaporation and secondary OA formation from
747 VOCs, IVOCs, and SVOCs.

748 Huang, R. J., Zhang, Y., Bozzetti, C., Ho, K. F., Cao, J. J., Han, Y., ... & Prévôt, A. S.
749 (2014). High secondary aerosol contribution to particulate pollution during
750 haze events in China. *Nature*, 514(7521), 218-222.

751 Koo, B., Knipping, E., & Yarwood, G. (2014). 1.5-Dimensional volatility basis set
752 approach for modeling organic aerosol in CAMx and CMAQ. *Atmospheric
753 Environment*, 95, 158-164.

754 Lane, T. E., Donahue, N. M., & Pandis, S. N. (2008). Simulating secondary organic
755 aerosol formation using the volatility basis-set approach in a chemical
756 transport model. *Atmospheric Environment*, 42(32), 7439-7451.

757 Li, J., Zhang, H., Li, L., Ye, F., Wang, H., Guo, S., ... & Hu, J. (2023). Modeling
758 Secondary Organic Aerosols in China: State of the Art and Perspectives.
759 *Current Pollution Reports*, 9(1), 22-45.

760 Li, H., Zheng, B., Lei, Y., Hauglustaine, D., Chen, C., Lin, X., ... & He, K. (2024).
761 Trends and drivers of anthropogenic NO_x emissions in China since
762 2020. *Environmental Science and Ecotechnology*, 21, 100425.

763 O'Brien, R.E. and Kroll, J.H. (2019). Photolytic aging of secondary organic aerosol:
764 Evidence for a substantial photo-recalcitrant fraction. *The journal of physical*
765 *chemistry letters*, 10(14), pp.4003-4009.

766 Pankow, J.F. and Asher, W.E., 2008. SIMPOL. 1: a simple group contribution method
767 for predicting vapor pressures and enthalpies of vaporization of
768 multifunctional organic compounds. *Atmospheric Chemistry and Physics*,
769 8(10), pp.2773-2796.

770 Pai, S. J., Heald, C. L., Pierce, J. R., Farina, S. C., Marais, E. A., Jimenez, J. L., ... &
771 Vu, K. (2020). An evaluation of global organic aerosol schemes using airborne
772 observations. *Atmospheric Chemistry and Physics*, 20(5), 2637-2665.

773 Pankow, J. F. (1994). An absorption model of the gas/aerosol partitioning involved in
774 the formation of secondary organic aerosol. *Atmospheric Environment*, 28(2),
775 189-193.

776 Pennington, E. A., Seltzer, K. M., Murphy, B. N., Qin, M., Seinfeld, J. H., & Pye, H.
777 O. (2021). Modeling secondary organic aerosol formation from volatile
778 chemical products. *Atmospheric Chemistry and Physics*, 21(24), 18247-18261.

779 Pennington, Elyse A., Yuan Wang, Benjamin C. Schulze, Karl M. Seltzer, Jiani Yang,
780 Bin Zhao, Zhe Jiang et al. "An updated modeling framework to simulate Los
781 Angeles air quality—Part 1: Model development, evaluation, and source
782 apportionment." *Atmospheric Chemistry and Physics* 24, no. 4 (2024):
783 2345-2363.

784 Pye, H. O. T., Chan, A. W. H., Barkley, M. P., & Seinfeld, J. H. (2010). Global
785 modeling of organic aerosol: the importance of reactive nitrogen (NO_x and
786 NO₃). *Atmospheric Chemistry and Physics*, 10(22), 11261-11276.

787 Pye, H.O., Pinder, R.W., Piletic, I.R., Xie, Y., Capps, S.L., Lin, Y.H., Surratt, J.D.,
788 Zhang, Z., Gold, A., Luecken, D.J. and Hutzell, W.T. (2013). Epoxide
789 pathways improve model predictions of isoprene markers and reveal key role

790 of acidity in aerosol formation. *Environmental Science & Technology*, 47(19),
791 pp.11056-11064.

792 Pye, H. O., Place, B. K., Murphy, B. N., Seltzer, K. M., D'Ambro, E. L., Allen, C., ...
793 & Stockwell, W. R. (2023). Linking gas, particulate, and toxic endpoints to air
794 emissions in the Community Regional Atmospheric Chemistry Multiphase
795 Mechanism (CRACMM). *Atmospheric Chemistry and Physics*, 23(9),
796 5043-5099.

801 Ramboll (2022). CAMx User's Guide, Version 7.20. Retrieved from
802 <https://www.camx.com/download/source/>, accessed on Feb. 15th, 2024

803 Robinson, A. L., Donahue, N. M., Shrivastava, M. K., Weitkamp, E. A., Sage, A. M.,
804 Grieshop, A. P., ... & Pandis, S. N. (2007). Rethinking organic aerosols:
805 Semivolatile emissions and photochemical aging. *Science*, 315(5816),
806 1259-1262.

807 Sarrafzadeh, M., Wildt, J., Pullinen, I., Springer, M., Kleist, E., Tillmann, R., Schmitt,
808 S.H., Wu, C., Mentel, T.F., Zhao, D. and Hastie, D.R. (2016). Impact of NO_x
809 and OH on secondary organic aerosol formation from β -pinene
810 photooxidation. *Atmospheric Chemistry and Physics*, 16(17), pp.11237-11248.

811 Sasidharan, S., He, Y., Akherati, A., Li, Q., Li, W., Cocker, D., ... & Jathar, S. H.
812 (2023). Secondary organic aerosol formation from volatile chemical product
813 emissions: Model parameters and contributions to anthropogenic aerosol.
814 *Environmental Science & Technology*, 57(32), 11891-11902.

815 Schell, B., Ackermann, I. J., Hass, H., Binkowski, F. S., & Ebel, A. (2001). Modeling
816 the formation of secondary organic aerosol within a comprehensive air quality
817 model system. *Journal of Geophysical Research: Atmospheres*, 106(D22),
818 28275-28293.

819 Shrivastava, M., Easter, R. C., Liu, X., Zelenyuk, A., Singh, B., Zhang, K., ... & Tiitta,
820 P. (2015). Global transformation and fate of SOA: Implications of low-
821 volatility SOA and gas-phase fragmentation reactions. *Journal of Geophysical
822 Research: Atmospheres*, 120(9), 4169-4195.

823 Shrivastava, M., Fast, J., Easter, R., Gustafson Jr, W. I., Zaveri, R. A., Jimenez, J.
824 L., ... & Hodzic, A. (2011). Modeling organic aerosols in a megacity:
825 comparison of simple and complex representations of the volatility basis set
826 approach. *Atmospheric Chemistry and Physics*, 11(13), 6639-6662.

827 Strader, R., Lurmann, F., & Pandis, S. N. (1999). Evaluation of secondary organic
828 aerosol formation in winter. *Atmospheric Environment*, 33(29), 4849-4863.

829 Tsimpidi, A. P., Karydis, V. A., Pandis, S. N., & Lelieveld, J. (2016). Global
830 combustion sources of organic aerosols: model comparison with 84 AMS
831 factor-analysis data sets. *Atmospheric Chemistry and Physics*, 16(14),
832 8939-8962.

833 Vitali, Bruno, Manuel Bettineschi, Arineh Cholakian, Dino Zardi, Federico Bianchi,
834 Victoria A. Sinclair, Johannes Mikkola et al. "Analysis of chemical and
835 transport processes of biogenic aerosols over the northern Apennines: insights
836 from the WRF-CHIMERE model." *Environmental Science: Atmospheres* 4, no.
837 9 (2024): 967-987.

838 Wildt, J., Mentel, T.F., Kiendler-Scharr, A., Hoffmann, T., Andres, S., Ehn, M.,
839 Kleist, E., Müsgen, P., Rohrer, F., Rudich, Y. and Springer, M. (2014).
840 Suppression of new particle formation from monoterpene oxidation by
841 NO_x. *Atmospheric Chemistry and Physics*, 14(6), pp.2789-2804.

842 WRF-Chem version 4.4 Users Guide. (2022).
843 https://ruc.noaa.gov/wrf/wrf-chem/Users_guide.pdf, accessed on Feb. 15th
844 2024.

845 Yarwood, G. and Tuite, K., 2024. Representing Ozone Formation from Volatile
846 Chemical Products (VCP) in Carbon Bond (CB) Chemical Mechanisms.
847 *Atmosphere*, 15(2), p.178.

848 Yu, H., Møller, K.H., Buenconsejo, R.S., Crouse, J.D., Kjaergaard, H.G. and
849 Wennberg, P.O., 2023. Atmospheric Photo-Oxidation of 2-Ethoxyethanol:
850 Autoxidation Chemistry of Glycol Ethers. *The Journal of Physical Chemistry*
851 *A*, 127(45), pp.9564-9579.

852 Zawadowicz, M. A., Lee, B. H., Shrivastava, M., Zelenyuk, A., Zaveri, R. A., Flynn,
853 C., ... & Shilling, J. E. (2020). Photolysis controls atmospheric budgets of
854 biogenic secondary organic aerosol. *Environmental Science & Technology*,
855 54(7), 3861-3870.

856 Zhang, Q. J., Beekmann, M., Drewnick, F., Freutel, F., Schneider, J., Crippa, M., ... &
857 Perrussel, O. (2013). Formation of organic aerosol in the Paris region during
858 the MEGAPOLI summer campaign: evaluation of the volatility-basis-set
859 approach within the CHIMERE model. *Atmospheric Chemistry and*
860 *Physics*, 13(11), 5767-5790.

861 Zhang, X., Cappa, C. D., Jathar, S. H., McVay, R. C., Ensberg, J. J., Kleeman, M. J.,
862 & Seinfeld, J. H. (2014). Influence of vapor wall loss in laboratory chambers
863 on yields of secondary organic aerosol. *Proceedings of the National Academy*
864 *of Sciences*, 111(16), 5802-5807.

- 865 Zhao, D., Schmitt, S. H., Wang, M., Acir, I. H., Tillmann, R., Tan, Z., ... & Mentel, T.
866 F. (2018). Effects of NO_x and SO₂ on the secondary organic aerosol
867 formation from photooxidation of α -pinene and limonene. *Atmospheric*
868 *Chemistry and Physics*, 18(3), 1611-1628.
- 869 Zhao, Y., Hennigan, C. J., May, A. A., Tkacik, D. S., de Gouw, J. A., Gilman, J. B., ...
870 & Robinson, A. L. (2014). Intermediate-volatility organic compounds: a large
871 source of secondary organic aerosol. *Environmental Science &*
872 *Technology*, 48(23), 13743-13750.
- 873 Zhao, B., Wang, S., Donahue, N. M., Jathar, S. H., Huang, X., Wu, W., ... &
874 Robinson, A. L. (2016). Quantifying the effect of organic aerosol aging and
875 intermediate-volatility emissions on regional-scale aerosol pollution in China.
876 *Scientific reports*, 6(1), 28815.